

# Modeling the hydrologic influence of subsurface tile drainage using the National Water Model

Prasanth Valayamkunnath<sup>1</sup>, David J Gochis<sup>1</sup>, Fei Chen<sup>1</sup>, Micheal Barlage<sup>2</sup>, and Kristie J. Franz<sup>3</sup>

<sup>1</sup>National Center for Atmospheric Research (UCAR)

<sup>2</sup>NCAR RAL

<sup>3</sup>Iowa State University

November 21, 2022

## Abstract

Subsurface tile drainage (TD) is a dominant agriculture water management practice in the United States (US) to enhance crop production in poorly-drained soils. Assessments of field- or watershed-level (<50 km<sup>2</sup>) hydrologic impacts of tile drainage are becoming common; however, a major gap exists in our understanding of regional (>105 km<sup>2</sup>) impacts of tile drainage on hydrology. The National Water Model (NWM) is a distributed 1-km resolution hydrological model designed to provide accurate streamflow forecasts at 2.7 million reaches across the US. The current NWM lacks tile drainage representation which adds considerable uncertainty to streamflow forecasts in tile-drained areas. In this study, we quantify the performance of the NWM with a newly incorporated tile drainage scheme over the heavily tile-drained Midwestern US. Implementing a tile drainage scheme enhanced the uncalibrated model performance by about 20% to 50% of the calibrated NWM (*Calib*). The calibrated NWM with tile drainage (*CalibTD*) showed enhanced accuracy with higher event hit rates and lower false alarm rates than *Calib*. *CalibTD* showed better performance in high-flow estimations as tile drainage increased streamflow peaks (14%), volume (2.3%), and baseflow (11%). Regional water balance analysis indicated that tile drainage significantly reduced surface runoff (-7% to -29%), groundwater recharge (-43% to -50%), evapotranspiration (-7% to -13%), and soil moisture content (-2% to -3%). However, infiltration and soil water storage potential significantly increased with tile drainage. Overall, our findings highlight the importance of incorporating the tile drainage process into the operational configuration of the NWM.



22 **Abstract**

23 Subsurface tile drainage (TD) is a dominant agriculture water management practice in the United  
24 States (US) to enhance crop production in poorly-drained soils. Assessments of field- or  
25 watershed-level (<50 km<sup>2</sup>) hydrologic impacts of tile drainage are becoming common; however,  
26 a major gap exists in our understanding of regional (>105 km<sup>2</sup>) impacts of tile drainage on  
27 hydrology. The National Water Model (NWM) is a distributed 1-km resolution hydrological  
28 model designed to provide accurate streamflow forecasts at 2.7 million reaches across the US.  
29 The current NWM lacks tile drainage representation which adds considerable uncertainty to  
30 streamflow forecasts in tile-drained areas. In this study, we quantify the performance of the  
31 NWM with a newly incorporated tile drainage scheme over the heavily tile-drained Midwestern  
32 US. Implementing a tile drainage scheme enhanced the uncalibrated model performance by  
33 about 20% to 50% of the calibrated NWM (*Calib*). The calibrated NWM with tile drainage  
34 (*CalibTD*) showed enhanced accuracy with higher event hit rates and lower false alarm rates than  
35 *Calib*. *CalibTD* showed better performance in high-flow estimations as tile drainage increased  
36 streamflow peaks (14%), volume (2.3%), and baseflow (11%). Regional water balance analysis  
37 indicated that tile drainage significantly reduced surface runoff (-7% to -29%), groundwater  
38 recharge (-43% to -50%), evapotranspiration (-7% to -13%), and soil moisture content (-2% to -  
39 3%). However, infiltration and soil water storage potential significantly increased with tile  
40 drainage. Overall, our findings highlight the importance of incorporating the tile drainage  
41 process into the operational configuration of the NWM.

## 42 **1. Introduction**

43 Agriculture management practices such as irrigation, fertilizer and pesticide application, and  
44 tillage are generally employed to enhance crop productivity and are crucial for global food  
45 production and food security. Agriculture subsurface drainage, often known as subsurface tile  
46 drainage, is a widely-used agriculture water management practice to improve crop growth in  
47 regions with shallow water tables or poorly drained soils. According to the United States  
48 Department of Agriculture (USDA) National Agricultural Statistics Service (NASS) Census of  
49 Agriculture 2017, about 22.48 million hectares (Mha) of croplands in the US are tile-drained,  
50 and 83.80% of the total tile-drained croplands of the US are concentrated in six Midwestern  
51 states (USDA-NASS, 2017) (Figure 1a), which is one of the world's most productive areas in  
52 terms of food and bioenergy, and it is located in the headwater regions of the Mississippi River  
53 (Ganter et al., 2014; Ray et al., 2013).

54 In general, tile drains are buried under the crop root zone to extract saturation water (or free  
55 water) from the soil, improve root-zone soil aeration and soil quality, reduce crop root diseases  
56 and soil erosion, allow for earlier planting and enhance crop yield (Figure 1b) (Du et al., 2005;  
57 Fausey, 2005; Fausey et al., 1987; Kornecki and Fouss, 2001). Furthermore, tile drainage is  
58 known to have a significant impact on watershed hydrology (Blann et al., 2009; King et al.,  
59 2014; Rahman et al., 2014; Thomas et al., 2016), because it depletes the free water from the root-  
60 zone soil layer, resulting in enhanced infiltration and reduced surface runoff, peak flows, and  
61 flooding (Golmohammadi et al., 2017; Rahman et al., 2014; Robinson and Rycroft, 1999; Skaggs  
62 et al., 1994). Tile drainage may also increase the watershed baseflow, annual runoff volume,  
63 instream pollutant concentrations, the timing and shape of the hydrograph, and the local and  
64 regional climate by modifying energy and water flux from croplands to the atmosphere (Blann et  
65 al., 2009; Eastman et al., 2010; Guo et al., 2018; Khand et al., 2017; King et al., 2014; Magner et  
66 al., 2004; Schilling et al., 2012; Schilling and Helmers, 2008; Schilling and Libra, 2003;  
67 Schottler et al., 2014; Thomas et al., 2016; Yang et al., 2017). However, the intensity and  
68 direction of the tile-drainage impact on hydrology depend on several field-specific factors such  
69 as soil properties, antecedent soil moisture storage, climatic conditions, topography, design of the  
70 tile drainage system, and tillage practices (Blann et al., 2009; King et al., 2014; Robinson, 1990;  
71 Robinson and Rycroft, 1999; Skaggs et al., 1994; Thomas et al., 2016; Wiskow and van der

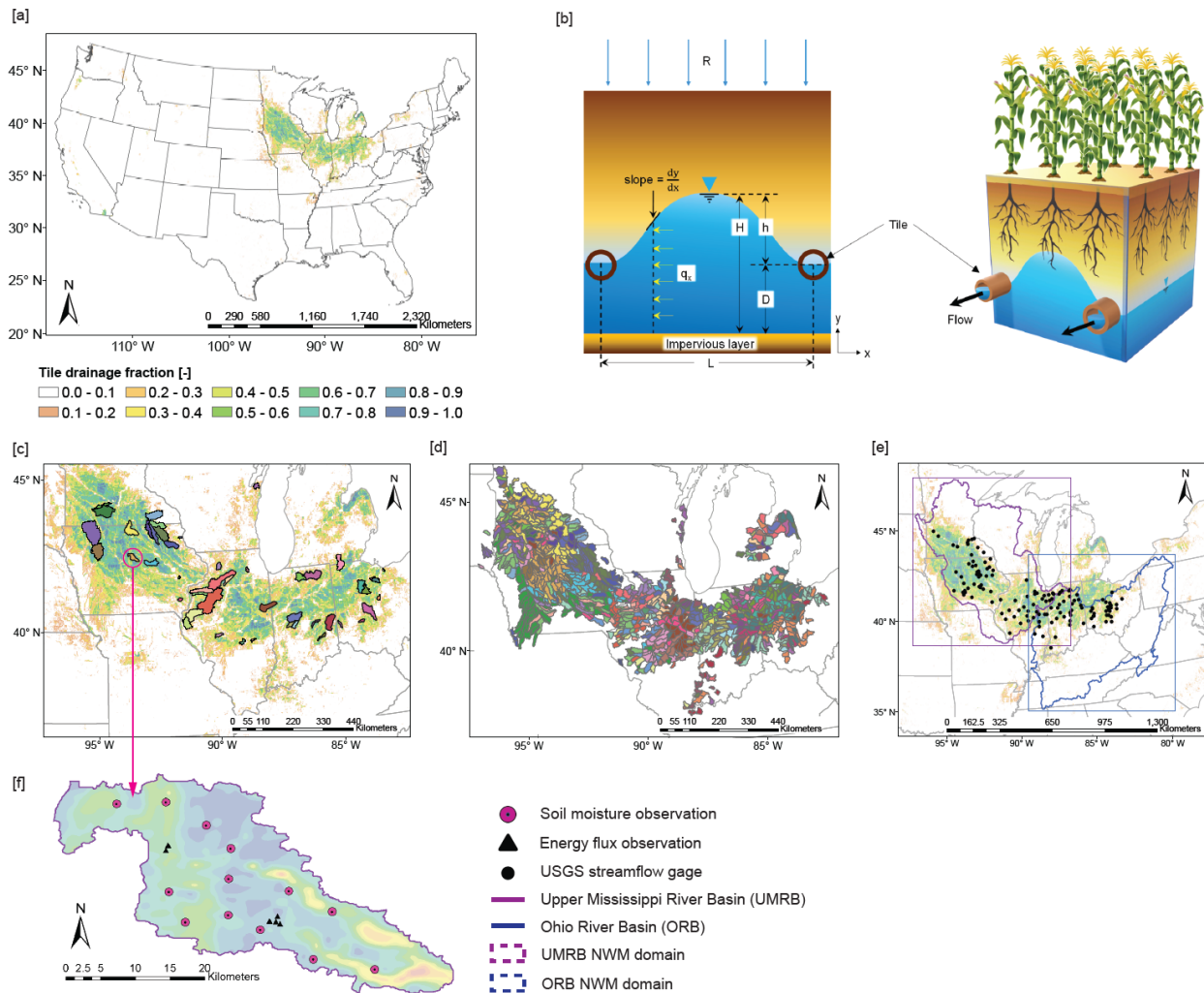
72 Ploeg, 2003). The above findings on the hydrologic impact of tile drainage are based on field-  
73 level or small watershed-scale (<50 km<sup>2</sup>) studies. A comprehensive understanding of regional-  
74 scale hydrology of tile-drainage is a major knowledge gap (Hansen et al., 2013; King et al.,  
75 2014; Thomas et al., 2016). Accurate modeling of tile drainage impacts on the continental or  
76 regional water cycle is a daunting challenge due to the lack of continental-scale high-resolution  
77 tile drainage data and an efficient, fully distributed, continental-scale hydrology model with a tile  
78 drainage scheme.

79 In the recent decade, the flood frequency and intensity have increased over the continental  
80 United States (CONUS), especially over the Central US (Mallakpour and Villarini, 2015). To  
81 provide flash flood forecasts and other hydrologic guidance with longer lead time and less  
82 uncertainties, the National Weather Service (NWS) Office of Water Prediction (OWP) of the  
83 National Oceanic and Atmospheric Administration (NOAA) developed a hydrologic modeling  
84 framework, the National Water Model (NWM), to simulate observed and forecast streamflow for  
85 about 2.7 million stream reaches of the CONUS. However, the NWM has considerable  
86 uncertainties in the streamflow prediction over the Midwestern US (Dugger et al., 2017; Karki et  
87 al., 2021). One of the reasons for the underperformance of the NWM can be the lack of  
88 representation of subsurface tile drainage hydrology in the NWM (Hansen et al., 2013). Field-  
89 level studies have already highlighted the importance of defining tile drainage within the  
90 hydrologic models to achieve accuracy in simulated water budget components over heavily tile-  
91 drained regions (Green et al., 2006; Hansen et al., 2013).

92 To address these shortfalls, in this study, we investigate the regional impact of tile drainage on  
93 the NWM performance in simulating streamflow over the upper Midwestern US by developing a  
94 new tile drainage scheme and implementing it into the NWM. We evaluate the NWM model  
95 performance with tile drainage regarding the streamflow simulation with and without NWM  
96 parameter calibration, and explore the influence of tile drainage on regional water budget and  
97 regional hydrology. In these simulations, we use the recently developed 30-meter resolution  
98 Agriculture Tile drainage data for the US (AgTile-US) (Valayamkunnath et al., 2020) to  
99 explicitly define the tile-drained croplands within the NWM.

100 In section 2, we describe the details of the study area, process descriptions of the NWM and the  
101 new tile drainage scheme, introduction to the input and evaluation data, calibration and

102 regionalization of model parameters, and details of model simulation experiments. Details of  
 103 hydrological and statistical analysis used in this study to evaluate the model performance are  
 104 presented in section 2.8. The results on the model performance evaluation, the impact of tile  
 105 drainage on energy and water balance components, comparison with parallel works,  
 106 perspectives, and limitations of the study are discussed in section 3.



107  
 108 **Figure 1.** The Study area. (a) The spatial distribution of tile drainage over the CONUS. The  
 109 color grading in (a) indicate the tile drainage area fraction on a 1-km NWM grid. (b) Schematic  
 110 representation of tile drainage and parameters of Hooghoudt’s tile drainage equation, (c) NWM  
 111 tile drainage calibration basins, (d) spatial distribution of regionalization HUC10s. In (d), color  
 112 represent corresponding donor basin for the NWM parameters in (c). (e) Represents the two  
 113 HUC2 basins identified for the regional NWM simulations. (f) The spatial distribution of soil  
 114 moisture and energy flux observations in the South Fork Iowa River watershed, Iowa.

115

## 116 2. Study area, modeling approach, and evaluation data

### 117 2.1 Study area description

118 Our investigation on the influence of tile drainage on the NWM performance and regional  
119 hydrology is based on the extensively tile-drained croplands of the upper Midwestern US (Figure  
120 1 and S1). Considering computational-resource constraints, we focus on two subdomains with  
121 extensive installations of tile drainage: The Upper Mississippi River Basin (UMRB) and the  
122 Ohio River Basin (ORB) (Figure 1e). According to the AgTile-US tile drainage data  
123 (Valayamkunnath et al., 2020), nearly 50% of total tile-drained croplands of the US are in the  
124 UMRB, which accounts for 24.58% of the geographical area of the UMRB and 48% of the total  
125 cropland area of the UMRB (Figure S1). Tile-drained croplands of ORB is about 17.2% of the  
126 total tile-drained area of the US. Approximately 41.27% of the ORB croplands are tile-drained,  
127 which covers 8.79% of the geographical area of the ORB. Together, UMRB and ORB account  
128 for nearly 67% of the total tile drainage area of the US. Generally, the croplands of the upper  
129 Midwestern region are characterized by moderately to very poorly drained soils and shallow  
130 water tables (Barlage et al., 2021; Valayamkunnath et al., 2020). During the 2013-2019 period,  
131 the annual average precipitation over UMRB and ORB are 1150 mm and 1370 mm, respectively.  
132 Both basins receive the majority of the annual rainfall during the summer (June-August) season.

### 133 2.2 The National Water Model (NWM)

134 The NWM is a joint development between National Center for Atmospheric Research (NCAR)  
135 and NOAA NWS to provide water prediction capabilities to advance resilience to water risks.  
136 The core of the NWM is the NCAR Weather Research and Forecasting Hydrologic (WRF-  
137 Hydro) model (Gochis et al., 2018). WRF-Hydro is a parallelized distributed hydrologic model  
138 that is designed to simulate the land surface hydrology and energy states at relatively high spatial  
139 resolution (usually 1-km or less). The NWM can either be forced offline (uncoupled) using  
140 prescribed atmospheric forcing variables or coupled to the Advanced Research version of the  
141 WRF (WRF-ARW) atmospheric model (Skamarock et al., 2008). Atmospheric forcing data  
142 required for the model operation include incoming shortwave radiation ( $Wm^{-2}$ ), incoming  
143 longwave radiation ( $Wm^{-2}$ ), specific humidity ( $kg\ kg^{-1}$ ), air temperature (K), surface pressure  
144 (Pa), liquid water precipitation rate ( $mm\ s^{-1}$ ), and near-surface wind (both u and y components,  $m$   
145  $s^{-1}$ ).

146 The NWM uses the Noah-MP land surface model (Niu et al. 2011) to resolve land surface  
147 processes and vertical fluxes of energy (sensible and latent heat, net radiation) and water (canopy  
148 interception, infiltration, infiltration-excess, deep percolation) within the soil column on a 1-km  
149 grid every 60 minutes. Infiltration excess, ponded water depth, and soil moisture are  
150 subsequently disaggregated from a 1-km Noah-MP grid to a high-resolution, 250-m, NWM  
151 routing grid using a time-step weighted method, and are then used in the subsurface and overland  
152 flow terrain-routing modules (Gochis et al., 2018).

153 Prior to the overland flow routing, the NWM subsurface flow module computes the subsurface  
154 lateral flow and resulting changes in the water table depth in the 2-m deep soil column using  
155 Dupuit–Forcheimer assumptions (Gochis et al. 2018). If subsurface lateral flow fully saturates a  
156 model grid, exfiltration is computed and added to the infiltration excess estimated by the Noah-  
157 MP and routed as surface runoff. Overland flow is calculated at a 10-seconds time-step using a  
158 fully unsteady, spatially explicit, diffusive wave routing formulation based on the steepest  
159 gradient around each grid point (Julien et al. 1995). See Gochis et al. (2018) for more details of  
160 the surface and subsurface routing schemes of NWM. As the surface flow reaches the grid  
161 identified as a channel, it is mapped to the vector channel network and routed downstream using  
162 Muskingum-Cunge channel routing formulation. In the NWM, vector channel networks are  
163 defined using National Hydrography Dataset (NHD) Plus Version 2 (NHDPlusV2) channel  
164 networks. A conceptual exponential bucket model is used to account for the contribution of  
165 baseflow to total streamflow in the NWM. Aggregated drainage from the Noah-MP soil column  
166 is mapped to a groundwater catchment corresponding to the NHDPlusV2 channel reach or  
167 catchment topology. Using an exponential storage-discharge function NWM estimates  
168 groundwater discharge for each NHDPlusV2 channel reach/catchment pair at hourly time steps  
169 (Gochis et al. 2018).

170 **Table 1.** Calibrated NWM parameters in V2.0. ('×' in the values denote that the calibration parameter is a multiplier on the default  
 171 value)

Parameter name	Description	Unit	Calibration value ranges (Minimum, Maximum)
BEXP	Pore size distribution index	dimensionless	(×0.40, ×1.90)
SMCMAX	Saturation soil moisture content (i.e., porosity)	volumetric fraction	(×0.80, ×1.20)
DKSAT	Saturated hydraulic conductivity	m s <sup>-1</sup>	(×0.20, ×10.00)
RSURFEXP	Exponent in the resistance equation for soil evaporation	dimensionless	(1.00, 6.00)
REFKDT	Surface runoff parameter. Increasing REFKDT decreases surface runoff	unitless	(0.10, 4.00)
SLOPE	Linear scaling of "openness" of bottom drainage boundary	0-1	(0.00, 1.00)
RETDEPRTFAC	Multiplier on retention depth limit	unitless	(0.10, 20000.00)
LKSATFAC	Multiplier on lateral hydraulic conductivity (controls anisotropy between vertical and lateral conductivity)	unitless	(10.00, 10000.00)
Zmax	Maximum groundwater bucket depth	mm	(10.00, 250.00)
Expon	Exponent controlling rate of bucket drainage as a function of depth	dimensionless	(1.00, 8.00)
CWPVT	Canopy wind extinction parameter for canopy wind profile formulation	m <sup>-1</sup>	(×0.50, ×2.00)
VCMX25	Maximum carboxylation at 25°C	umol m <sup>-2</sup> s <sup>-1</sup>	(×0.60, ×1.40)
MP	Slope of Ball-Berry conductance-to-photosynthesis relationship	unitless	(×0.60, ×1.40)
MFSNO	Melt factor for snow depletion curve; larger value yields a smaller snow cover fraction for the same snow height	dimensionless	(×0.25, ×2.00)
TD_SPAC	Tile drain spacing	m	(×0.25, ×2.00)

172

173 In this study, we use NWM version 2.0 (V2.0). The NWM has parameters that can be input into  
174 the model as tables and grids and can be tuned or calibrated depending on the research  
175 requirements. The list of important NWM V2.0 parameters identified by the NCAR to regionally  
176 calibrate NWM (Dugger et al., 2017; Gochis et al., 2019) are listed in Table 1.

### 177 **2.3 Tile drainage scheme**

178 The current NWM lacks the representation of subsurface tile drainage. To compute tile drainage  
179 runoff in the NWM, we implemented a simple analytic solution for subsurface flow to drains  
180 based on Hooghoudt's tile-drainage model (Hooghoudt 1940; Ritzema, 1994). Hooghoudt's  
181 model computes steady-state flow into the tile by applying Dupuit-Forchheimer assumptions for  
182 horizontal flow in an unconfined aquifer and Darcy's Equation. The Hooghoudt's tile-drainage  
183 model is computationally simple, and therefore is commonly used to compute the tile drainage  
184 runoff in other models, especially in the DRAINMOD model (Skaggs, 1980) and Soil and Water  
185 Assessment Tool (SWAT) model (Arnold et al., 1999; Guo et al., 2018; Moriasi et al., 2012).  
186 Hooghoudt's steady-state equation that is implemented in the NWM is represented by Equation  
187 1.

$$188 \quad q = \frac{8KDh + 4Kh^2}{L^2} \quad (1)$$

189 Where,  $q$  is the drainage discharge ( $\text{m d}^{-1}$ ),  $K$  is the hydraulic conductivity of the soil ( $\text{m d}^{-1}$ ),  $L$  is  
190 the distance between tile drains,  $h$  is mid-point water table height above the tile drains (m) and  $D$   
191 is the height of tile drain from the bottom impervious layer (m) (Figure 1b). If the tile drain is  
192 sufficient distance above the impervious layer, the streamlines will converge towards the tile  
193 drain and thus no longer be horizontal. This results in longer flowlines and extra head loss. To  
194 meet the Dupuit-Forchheimer assumptions of vertical equipotential lines and horizontal flow  
195 streamlines and to correct for convergence head loss near the tile drains,  $D$  in Equation (1) is  
196 replaced with the equivalent depth term ( $d_e$ ) (Moody, 1967). The equivalent depth ( $d_e$ ) represents  
197 the imaginary thinner soil layer through which the same amount of water will flow per unit time  
198 as in the actual situation (Ritzema, 1994). The value of  $d_e$  can be obtained using the analytical  
199 equations developed from Hooghoudt's solutions as a function of  $L$ ,  $D$ , and radius ( $r$ ) of tile  
200 drain (Moody, 1967) that are provided in Ritzema (1994).

201 Hooghoudt's model is a suitable option for the NWM framework because it considers most  
202 factors determining subsurface flow into tiles:  $K$ ,  $L$ ,  $D$ , soil profile depth, and water table  
203 elevation. Parameter  $K$  is already defined in the NWM. Default values of  $D$ ,  $r$  and  $L$  are  
204 prescribed based on values reported by previous studies (Guo et al., 2018; Huffman et al., 2011;  
205 Moriasi et al., 2012; Panuska 2020; Schilling and Helmers 2008; Singh et al. 2006; 2007; Singh  
206 and Helmers 2008). The water table depth term,  $h$  is diagnosed at each model time-step using the  
207 degree of soil saturation simulated by Noah-MP. The tile drainage estimated by the Noah-MP at  
208 1-km is then disaggregated onto a 250-m routing grid. In the NWM channel routing module, the  
209 lateral tile drainage runoff is mapped to the nearest vector channel network and routed  
210 downstream using Muskingum-Cunge channel routing formulation. We used the 30-meter  
211 resolution AgTile-US (Valayamkunnath et al., 2020) tile drainage map re-gridded to a 1-km  
212 NWM grid to define the tile-drained area within the model (Figure 1a).

## 213 **2.4 Data**

### 214 **2.4.1 Observations**

215 The study used hourly streamflow measurements from 188 United States Geological Survey  
216 (USGS) streamflow gages spanning across the heavily tile-drained croplands of the Upper  
217 Midwestern US (Figure 1c and 1e). These gages are selected from a list of USGS gages over the  
218 study area based on two criteria: 1) if the missing data in the streamflow time series is less than  
219 20%, and 2) tile drainage fraction within the catchment is greater than 10%. To further examine  
220 the influence of tile drainage on evapotranspiration and soil moisture, we used *in-situ*  
221 measurements from the South Fork Iowa River watershed collected by the Agriculture Research  
222 Service of the United States Department of Agriculture (Coopersmith et al., 2015; 2021) (Figure  
223 1f), including six sites with hourly flux measurements (latent and sensible heat fluxes) and 12  
224 sites with daily soil moisture measurements. To validate the NWM simulated energy fluxes, we  
225 used daytime (9 am - 5 pm local time) hourly flux measurements.

### 226 **2.4.2 Forcings for NWM**

227 To drive the NWM, we used Analysis of Record for Calibration (AORC) high-resolution (1-km),  
228 near-surface, hourly meteorological forcing data (Kitzmilller et al., 2018) is available from 1979  
229 to the present for the CONUS. The AORC delivers hourly accumulated precipitation and other  
230 meteorological surface parameters on a  $0.0083^\circ$  grid mesh. It provides superior temperature and

231 precipitation data than the widely-used National Land Data Assimilation System Version 2  
232 (NLDAS2) meteorological forcings (Feng et al., 2019; Xia et al., 2012). The AORC is being  
233 used as the primary source of forcing data for the calibration of the operational NWM by NCAR  
234 and OWP (Feng et al., 2019). To derive high-resolution hourly precipitation, the AORC used  
235 different sources of precipitation data such as Livneh (Livneh et al., 2013), NLDAS2 (Xia et al.,  
236 2012), Stage IV (Lin and Mitchell, 2005), radar inputs, CMORPH (Joyce et al., 2004), and  
237 Climate Forecast System Reanalysis (CFSR) (Saha et al., 2014). For temperature, Livneh,  
238 NLDAS2, and Parameter Regression on Independent Slopes Method (PRISM) (Daly et al., 2002)  
239 data were used. See Kitzmiller et al. (2018) for more details on the AORC meteorological  
240 forcings. Other variables in AORC, including specific humidity, 10-m above ground wind  
241 components, terrain-level pressure, surface downward shortwave (solar) radiation flux, and  
242 longwave (infrared) radiation flux, were derived from NLDAS2.

243 Additional static data used for the NWM simulations include NLCD land cover (reclassified on  
244 to USGS 27-class, 30-arc second), Hybrid STATSGO/FAO Soil Texture (19-class, 30-arc  
245 second), and AgTile-US tile drainage map (30-m).

## 246 **2.5 Calibration of the NWM with a tile drainage scheme**

247 The key elements of an automated calibration workflow are the calibration data, objective  
248 function, and the optimization algorithm employed to optimize the objective function in order to  
249 minimize the model error (Gupta et al., 1998; Singh and Woolhiser 2002; Tolson and Shoemaker  
250 2007). Following the actual NWM calibration procedure (Gochis et al., 2019), we calibrated  
251 NWM against the USGS hourly streamflow data. The objective function used for the calibration  
252 is provided in Equation 2. The standard Nash–Sutcliffe Efficiency (NSE) emphasizes the high  
253 flow performance of the model due to squared error terms. However, combining NSE of log-  
254 transformed streamflow with standard NSE provides an additional emphasis on low flows to  
255 account for background model bias. During calibration, the objective function will be minimized.

$$256 \quad \text{Objective function} = 1 - \frac{(NSE + NSE_{LOG})}{2} \quad (2)$$

257 Here,  $NSE$  is the Nash-Sutcliffe Efficiency and  $NSE_{LOG}$  is the Log-transformed NSE (see Table  
258 2 for more details).

259 **Table 2.** Evaluation metrics used for the performance evaluation of the NWM.

Metrics	Equation	Description
Pearson's Correlation (COR)	$r = \frac{\sum_{i=1}^n (m_i - \bar{m})(o_i - \bar{o})}{\sqrt{\sum_{i=1}^n (m_i - \bar{m})^2 \sum_{i=1}^n (o_i - \bar{o})^2}}$	Here, $m_i$ and $\bar{m}$ are the $i^{\text{th}}$ value and mean of NWM simulated streamflow, respectively. $o_i$ and $\bar{o}$ are same as above but for the observation, and $n$ is the length of streamflow series. Values greater than 0.5 are considered acceptable levels of performance. COR is used to capture the flow timing (Benesty et al., 2009; Moriasi et al., 2007). (Optimal value = 1)
Root mean squared error (RMSE)	$RMSE = \sqrt{\sum_{i=1}^n (m_i - o_i)^2 / n}$	All terms have same meaning as above. But RMSE is used to capture the flow magnitude. (Optimal value = 0)
Percent bias (Bias)	$Bias = \frac{\sum_{i=1}^n (m_i - o_i) \times 100}{\sum_{i=1}^n o_i}$	All terms have same meaning as above. But Bias is used to capture the flow magnitude. (Optimal value = 0)
Nash-Sutcliffe Efficiency (NSE)	$NSE = 1 - \left[ \frac{\sum_{i=1}^n (o_i - m_i)^2}{\sum_{i=1}^n (o_i - \bar{o})^2} \right]$	All terms have same meaning as above. Values between 0.0 and 1.0 are generally viewed as acceptable levels of performance. NSE can capture the flow timing and magnitude errors of the high flows (Moriasi et al., 2007; Nash and Sutcliffe, 1970). (Optimal value = 1)
Log-transformed Nash-Sutcliffe Efficiency (NSE <sub>LOG</sub> )	$NSE_{LOG} = 1 - \left[ \frac{\sum_{i=1}^n (\log(o_i) - \log(m_i))^2}{\sum_{i=1}^n (\log(o_i) - \overline{\log(o_i)})^2} \right]$	All terms have same meaning as above. Values between 0.0 and 1.0 are generally viewed as acceptable levels of performance. NSE <sub>LOG</sub> can capture the flow timing and magnitude errors of the low flows (Moriasi et al., 2007). (Optimal value = 1)
Weighted NSE (NSE <sub>WT</sub> )	$NSE_{WT} = (NSE + NSE_{LOG}) / 2$	All terms have same meaning as above. Values between 0.0 and 1.0 are generally viewed as acceptable levels of performance. NSE <sub>WT</sub> is used to capture flow timing and magnitude errors for low flows and high flows. (Moriasi et al., 2007). (Optimal value = 1)
Kling-Gupta Efficiency (KGE)	$KGE = 1 - \sqrt{(r - 1)^2 + \left(\frac{\sigma_m}{\sigma_o} - 1\right)^2 + \left(\frac{\bar{m}}{\bar{o}} - 1\right)^2}$	Here, $\sigma_m$ and $\sigma_o$ are standard deviations in simulated and observed streamflow, respectively and other terms have same meaning as above. The range $-0.41 < KGE \leq 1$ could be considered as reasonable levels model performance. KGE is used to capture timing and magnitude errors. (Gupta et al., 2009; Knoben et al., 2019)

261 As in the official calibration strategy of the NWM V2.0, the Dynamically Dimensioned Search  
262 (DDS) algorithm (Tolson and Shoemaker, 2007) is used in this study to optimize the objective  
263 function. The algorithm is designed to scale the search in model parameter space to the user-  
264 defined maximum number of iterations. The algorithm searches globally in its initial iterations  
265 and then localizes the searches as the iterations approach the user-defined limit. The transition  
266 from global to local search is attained by dynamically and probabilistically reducing the search  
267 dimension in the neighborhood. See Tolson and Shoemaker (2007) for more details on DDS. In  
268 this study, the maximum number of iterations is set to 300 for the NWM calibration.

269 Since the NWM simulations are data-, time-, and computationally-intensive, calibrating it for the  
270 large river basins of the US in a single experiment is a cumbersome task. According to Feng et  
271 al. (2019), about 1469 basins across the CONUS are identified from USGS GAGES II reference  
272 basins, California Department of Water Resources (CADWR) basins, and NOAA NWS River  
273 Forecast Centers (RFC) basins for the CONUS-scale calibration of the NWM V2.0. Calibration  
274 basins are selected based on basin size, completeness of the streamflow observation record,  
275 distribution within ecoregions level III (Omernik JM. 1995) and hydrograph characteristics in  
276 comparison to other basins in the region. A basin is selected if the basin area is between 10 km<sup>2</sup>  
277 and 20,000 km<sup>2</sup>, streamflow data completeness is at least 50% for the calibration period, and the  
278 basin has minimal human interventions (i.e., dams, road density, etc.) (Feng et al., 2019). To  
279 calibrate NWM for the UMRB and ORB, we used a subset of 49 basins from V2.0 calibration  
280 basins that have the tile-drainage area greater than or equal to 10% of the basin area (Figure 1c).

281 Before performing the calibration, we spin-up NWM for the selected 49 basins, separately, from  
282 October 1, 2007, through October 1, 2019 period using the default model parameters. Using the  
283 model state of October 1, 2019, as the “warm start,” we executed the model calibration from  
284 October 1, 2007, through October 1, 2013. A separate 1-year spin-up from October 1, 2007,  
285 through September 30, 2008, is considered for each iteration to match the model state to current  
286 conditions and suppress most instabilities from parameter changes. The critical parameters of the  
287 NWM (V2.0) related to soil, vegetation, runoff, snow, and groundwater and their description are  
288 provided in Table 1 along with the most sensitive tile-drainage model parameter, the tile spacing  
289 (L) parameter (Moriassi et al., 2012; Sammons et al., 2015; Guo et al., 2018). Using the best  
290 parameters determined by the DDS algorithm, we ran the NWM from October 1, 2007, through

291 October 1, 2019. Model outputs for the water years 2007-2013 are discarded as spin-up and  
292 calibration periods, and then we evaluated the model for all the 49 basins over the period  
293 October 1, 2013, to October 1, 2019.

## 294 **2.6 Regionalization of calibrated NWM parameters**

295 The total area of the calibrated basins is less than 10% of the area of UMRB and ORB combined.  
296 To compare the NWM performance with tile drainage and to quantify impacts of tile drainage on  
297 regional hydrology, regional NWM simulation experiments are necessary. To execute the NWM  
298 for regional domains presented in Figure (1e), appropriate parameters are required to be assigned  
299 for each 1-km model grid cell in the study domain. The purpose of the parameter regionalization  
300 is to transfer parameters from the calibration basins (donors) to the uncalibrated basins or 1-km  
301 model grids (receiver) (Beck et al., 2016; He et al., 2011; Hrachowitz et al., 2013; Razavi and  
302 Coulibaly, 2013). The most critical parts of the parameter regionalization process are identifying  
303 donor basins for uncalibrated areas and choosing an optimal regionalization approach. We used  
304 the regionalization based on maximum hydrological similarity (or minimum hydrologic distance)  
305 to identify donor basins for uncalibrated areas (Beck et al., 2016; Garambois et al., 2015; Sellami  
306 et al., 2014; Singh et al., 2014; Wallner et al., 2013). It is reasonable to assume that basins with  
307 similar climate, topography, vegetation, geology and soil properties have identical NWM  
308 parameters and produce similar hydrological responses. The hydrologic similarity or hydrologic  
309 distance is measured by the Gower's distance metric (Gower, 1971).

310 To calculate the Gower's distance between donor and receiver basins, we considered several  
311 attributes (see Table 3) based on the Hydrological Landscape Region (HLR) concept (Liu et al.,  
312 2008; Winter, 2001; Wolock et al., 2004). Before using the Gower's distance metric, we  
313 conducted a principal component analysis (PCA) to remove potential correlation between the  
314 basin attributes. Each basin attribute is scaled to [-1, 1] by subtracting the mean and then  
315 dividing by the standard deviation before the PCA. We used the following equation to quantify  
316 the Gower's distance,

$$317 \quad S_{ij} = \frac{\sum_{k=1}^n S_{ijk} \delta_{ijk}}{\sum_{k=1}^n \delta_{ijk}} \quad (3)$$

318 **Table 3.** Basin attributes used for characterizing hydrologic similarity in NWM 2.0 with tile drainage scheme

Category	Attribute	Notes
Landform	Percent flatland (total)	Total percent cover of flatland in the basin; flatland refers to areas with a slope of less than 0.01
	Percent flatland (upland)	Upland refers to areas above the middle elevation of the basin
	Percent flatland (lowland)	Lowland refers to areas below the middle elevation of the basin
	Relief	Difference between the highest and lowest elevations
	Circularity index	The ratio of the basin's area over the area of a circle with the same length of perimeter as the basin
Soil and geology	Percent sand	Mean percentage of sand in the soil column (upper 2m)
	Percent clay	Mean percentage of clay in the soil column (upper 2m)
	Depth to bedrock	Average thickness of soil
Land cover	Percent forest	Percent cover of forest (all types) in the basin
	Percent cropland	Percent cover of cropland (all types) in the basin
	Percent urban	Percent cover of urban areas in the basin
	Percent tile drainage	Percent cover of tile drained cropland in the basin
Climate	Feddema moisture index (FMI)	$1 - (\text{PET}/\text{P})$ (if $\text{P} \geq \text{PET}$ ) or $(\text{P}/\text{PET}) - 1$ (if $\text{P} < \text{PET}$ ), where P & PET are annual mean precipitation and potential evapotranspiration, respectively. See Feddema (2005) and Leibowitz et al. (2016) for more details.

319

320

321 Where,  $S_{ijk}$  is the distance for variable  $k$  between a donor ( $i$ ) and a receiver ( $j$ ) and  $\delta_{ijk}$  is the  
322 weight on variable  $k$ . For numerical variables, values of  $S_{ijk}$  are estimated as the absolute  
323 difference in the values of variable  $k$  between  $i$  and  $j$ , normalized by the range of variable  $k$  over  
324 all observations. For categorical variables,  $S_{ijk}$  is assigned to 1 if  $i$  and  $j$  are equal on variable  $k$   
325 and 0 if they are not. The variables used in Equation (3) are the scores of the principal  
326 components and weights ( $\delta_{ijk}$ ) are calculated based on the percentages of the total variance  
327 explained by individual principal components. The receiver basins depicted in Figure (1d) are  
328 extracted from USGS 10-digit Hydrologic Unit Code (HUC10) dataset. We selected 939 HUC10  
329 basins over the upper Midwestern US with at least 10% tile drainage (i.e., 10% tile drainage  
330 based on the total basin area) to regionalize the calibrated NWM parameters. For each HUC10  
331 basin, we calculated Gower's distance from all the 49 calibration basins, identify a donor basin  
332 based on minimum Gower's distance (i.e., maximum hydrologic similarity) and spatial distance  
333 from the HUC10 basin, and finally transferred all the parameters to the HUC10 basins from their  
334 respective donor basin. Using the shapefile of HUC10 basins and the NWM 1-km geogrid, we  
335 mapped the parameters to the 1-km model domain. For areas with no tile drainage, we used the  
336 parameters from the official NWM V2.0 calibration experiment by NCAR and OWP.

## 337 **2.7 Simulation experiments**

338 To examine the impact of tile drainage on the NWM performance and land surface hydrology,  
339 we conducted the following NWM simulations for the UMRB and ORB regional domains.

- 340 a. *Default*: default NWM V2.0 without parameter calibration
- 341 b. *DefaultTD*: as in *Default*, but including the tile-drainage model
- 342 c. *Calib*: NWM V2.0 with calibrated parameters, mimicking the operational NWM
- 343 d. *CalibTD*: as in *Calib* but using the tile-drainage model with calibrated tile-space  
344 parameter.

345 Similar to the calibration experiment, we spin-up all the four regional NWM experiments from  
346 October 1, 2012, through October 1, 2019, before performing the analysis run. Using October 1,  
347 2019 model state as the initial condition, we re-run the model from October 1, 2012, through  
348 October 1, 2019. The first water year (i.e., the water year 2012) model outputs are discarded

349 from the analysis as we use this as an additional model spin-up period. Simulated streamflow  
350 from model outputs is extracted for 139 USGS gage locations (Figure 1e). The results presented  
351 in this study for the UMRB and ORB regional domains are only for October 1, 2013, through  
352 October 1, 2019 period.

## 353 **2.8 Analysis**

354 The analyses conducted in this study to evaluate the model performance include hydrograph  
355 analysis and statistical analysis using various statistical performance metrics provided in Table 2.  
356 We evaluated the model simulated high flows, low flows, and streamflow events with  
357 observations using hydrograph analysis. We derived high flows and low flows based on observed  
358 streamflow quantiles. We split the observed and model estimated streamflow time series into 99  
359 segments based on streamflow quantiles ranging from 1 to 100% for every observation. Low  
360 flow is defined as streamflow below the median (50th quantile), and high flow is streamflow  
361 above the median (see Figure S2 in the supporting information for graphical explanations). For  
362 each quantile segment of the streamflow series, we estimated the model performance using  
363 metrics listed in Table 3. To identify streamflow events, we use a recently developed R package  
364 called “RNWMStat” (<https://github.com/NCAR/RNWMStat>) (Valayamkunnath et al., 2020).  
365 RNWMStat can detect and match streamflow events from the observed and simulated  
366 streamflow series.

367 The event detection algorithm in the RNWMStat follows a two-step procedure: first, the  
368 algorithm smooths the streamflow time series (simulated or observed) using the local weighted  
369 regression smoothing (LOESS) technique to remove high-frequency noises in the hydrographs;  
370 second, it determines the start, peak, and endpoints of streamflow events from the first derivative  
371 (i.e., rate of change) of smoothed streamflow series and remapped on to the original streamflow  
372 series. We matched a simulated streamflow event with an observed event if the simulated peak of  
373 an event is within the observed event (i.e., between the start and endpoints of an observed event).  
374 For the matched events, we estimate peak bias (%), timing error of peak streamflow (hours),  
375 event hit rate (%), and false alarm rate (%). Hit rate indicates the percentage of observed events  
376 that the model predicts, and false alarm rate is the percentage of model events that are not  
377 observed. For the event-based analysis, we used only the events with their peak greater than or  
378 equal to the 90<sup>th</sup> percentile of streamflow. We used the Wilcoxon signed-rank test at 5%

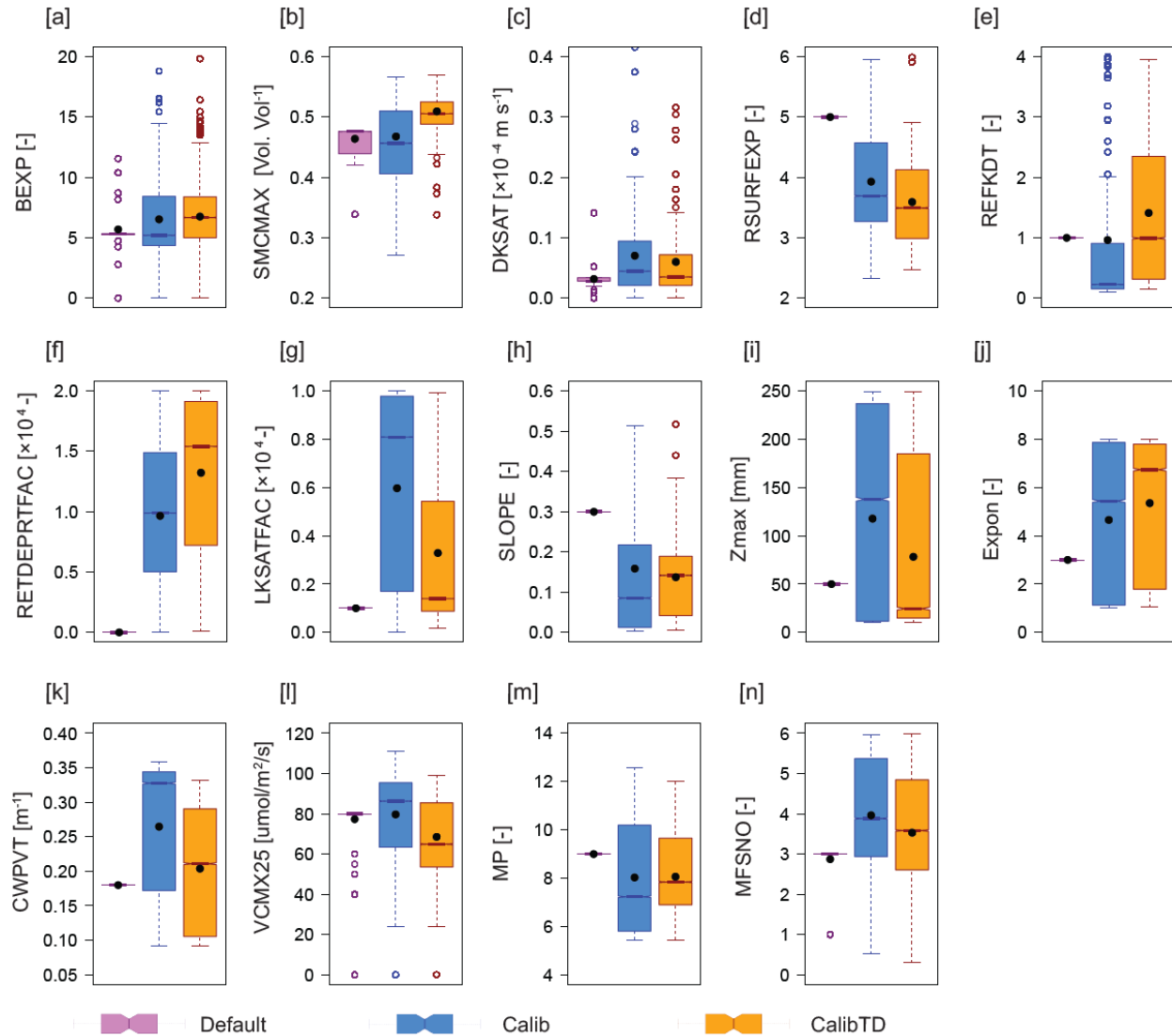
379 significance level to quantify the statistical significance of the median changes in the NWM  
380 performance. The estimated p-values are provided in Table S1 to Table S3.

### 381 **3. Results**

#### 382 **3.1 NWM calibration and parameter estimation**

383 The distributions of 14 sensitive parameters (Dugger et al., 2017; Gochis et al., 2019) from the  
384 *Default*, *Calib*, and *CalibTD* are presented in Figure 2. The physical meanings of these  
385 parameters are presented in Table 1. The new tile drainage scheme substantially altered the  
386 distributions of the NWM parameters. In *CalibTD*, the soil column is relatively water-absorbing  
387 or wetter than *Default* and *Calib*, because of its higher median values of pore size distribution  
388 index (BEXP) and soil porosity (SMCMAX). We observed a significant reduction in direct soil  
389 evaporation (RSURFEXP) and increase in infiltration (REFKDT) and surface water retention  
390 depth (RETDEPRTFAC) in *CalibTD* ( $p < 0.05$ ). Additionally, the degree of anisotropy in the  
391 soil saturated hydraulic conductivity (LKSATFAC) is greatly reduced ( $p < 0.05$ ) in *CalibTD*  
392 compared to *Calib*. However, the estimated LKSATFAC for *CalibTD* is significantly higher  
393 compared to *Default* ( $p < 0.05$ ). Furthermore, the degree of openness in the bottom drainage  
394 boundary (SLOPE) is slightly higher in *CalibTD* compared to *Calib*.

395 Based on STATSGO2 soil data, the dominant soil types of the study region are loam, silty clay  
396 loam, and silt loam (Miller and White, 1998; USDA-NRCS, 2012). Overall, the *CalibTD*  
397 parameters ranges are acceptable for the study region with a managed agriculture and above-  
398 listed soil types (Clapp and Hornberger 1978; Lipiec et al., 2006; Livneh et al., 2015; Ma et al.,  
399 2007; Miller and White, 1998). The distributions of the NWM parameters presented in Figure 2  
400 suggest that *CalibTD* creates favorable conditions for low surface runoff rates, high infiltration  
401 rates, a saturated soil column, and a shallow water table compared to *Calib* (Kalita et al., 2007).



402

403 **Figure 2.** The distributions of the NWM parameters from *Default*, *Calib* and *CalibTD*  
 404 experiments.

405

406 **3.2 NWM performance evaluation: calibration and validation periods**

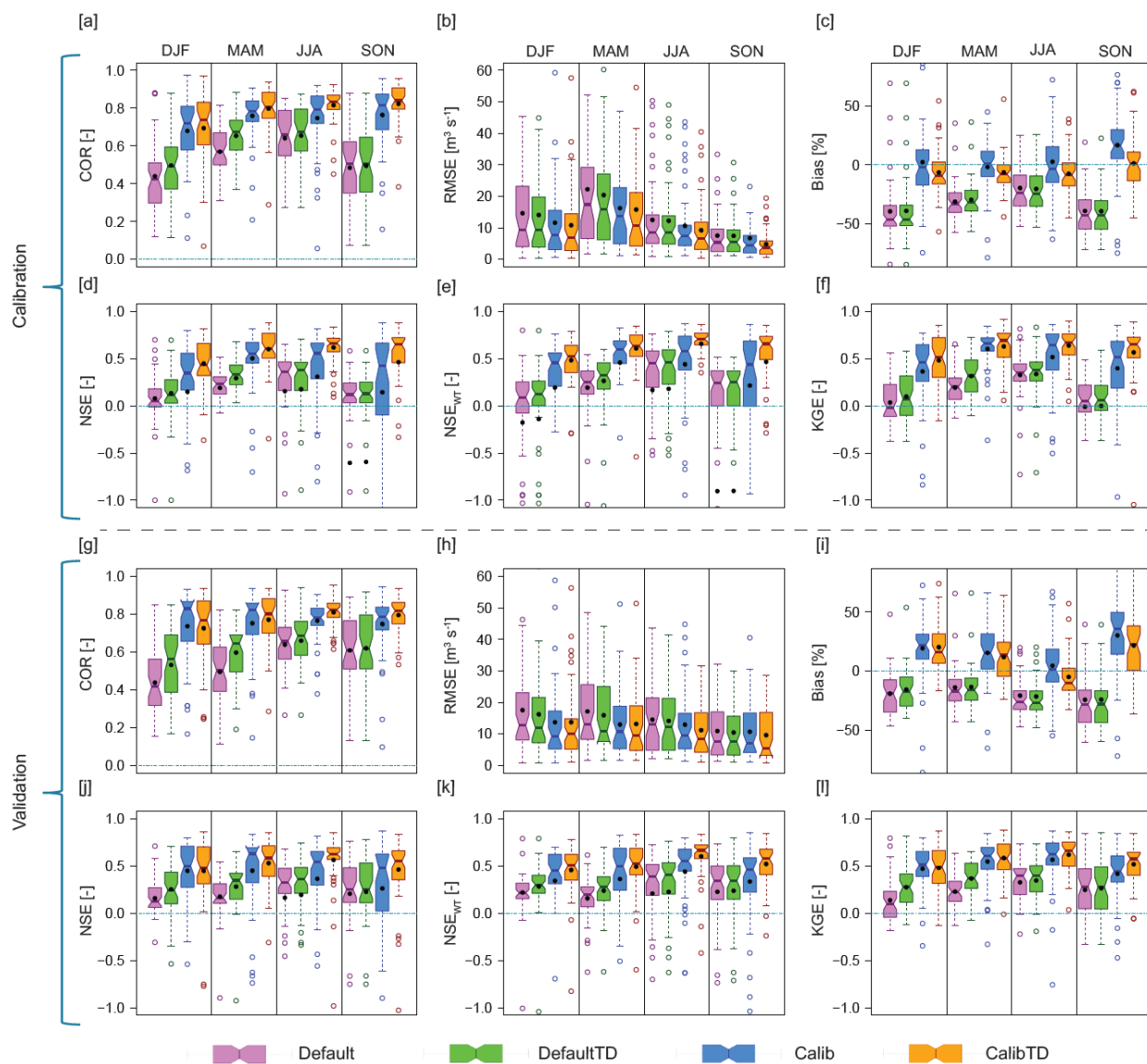
407 Seasonal distributions of NWM performance evaluation metrics for calibration and validation  
 408 periods are depicted in Figure 3. Representing the tile drainage process in the NWM improves  
 409 the model performance during the calibration period (Figure 3a-f). Examining the *DefaultTD*  
 410 model evaluation metrics indicated significant improvements in COR, NSE, NSE<sub>WT</sub>, and KGE  
 411 during all seasons than *Default* ( $p < 0.05$ ). Furthermore, the median and spread of RMSE are  
 412 considerably reduced in *DefaultTD* during all seasons than *Default*. There are no considerable

413 differences in the estimated Bias between *Default* and *DefaultTD*. Overall, *DefaultTD*  
414 performance is halfway between *Default* and *Calib*. That is, incorporating tile-drainage modeling  
415 into NWM using default parameters (i.e., *DefaultTD*) enhanced the NWM performance by 20%  
416 to 50% of the improvements attained by the fully-calibrated NWM (or *Calib*) from *Default* (e.g.,  
417 for spring, the median NSE improved from 0.22 (*Default*) to 0.55 (*Calib*) in the non-tiled model,  
418 and from 0.22 to 0.33 in the *Default* versus *DefaultTD*). The improvement seen in the *DefaultTD*  
419 emphasizes the benefit of incorporating more physical process representation into hydrologic  
420 models, rather than relying on calibration to compensate for model deficiencies, which ultimately  
421 leads to uncertainty in model reliability across time (Andréassian, 2012; Gharari et al., 2014;  
422 Ljung, 1999).

423 Compared to *Default*, the biggest improvement was brought by the *Calib* based on all the metrics  
424 we considered (Figure 3a-f and Table S1). However, examining NSE, NSE<sub>WT</sub>, and KGE  
425 indicated that *Calib* has considerable discrepancies in the simulated streamflow over many  
426 calibration basins. Based on the valid ranges of evaluation metrics presented in Table 2, the  
427 performance of *Calib* is unacceptable in about 18%, 6%, 20%, and 30% of the calibration basins  
428 during winter, spring, summer, and fall, respectively (Figure 3d-f). In *CalibTD*, these  
429 underperforming basin percentage is reduced to 4%, 2%, 0%, and 6%, respectively for winter,  
430 spring, summer, and fall. Additionally, we observed higher metrics medians with lower  
431 variabilities for the *CalibTD*. Seasonal analysis indicated that the NWM performance is best  
432 during summer and fall. It is due to the high amount of precipitation and streamflow during these  
433 seasons. Overall, calibration of the NWM with a tile drainage scheme (i.e., *CalibTD*)  
434 significantly improved the model performance than other model experiments ( $p < 0.05$ ) (Figure  
435 3a-f and Table S1). Despite the improvements seen in the *DefaultTD*, it was necessary to  
436 calibrate to attain improved model performance.

437 Using the best parameters identified by the optimization algorithm, we executed the model for  
438 the validation period. As shown in Figure 3g-i, the *DefaultTD* outperformed *Default*. The  
439 improvements in NSE, NSE<sub>WT</sub>, KGE, COR for the *DefaultTD* are significant ( $p < 0.05$ ) during  
440 winter and spring compared to *Default*. Similarly, *CalibTD* performed better than *Calib* during  
441 the validation period (Figure 3g-I and Table S2), especially during summer and fall. Examining,  
442 COR, NSE, and KGE indicated that *CalibTD* performed slightly worse during winter and spring

443 because it failed to reproduce the flow timings and peaks accurately. Biases in the timing and  
 444 intensity of snowmelt can be another reason (Suzuki and Zupanski, 2018). Overall, incorporating  
 445 the tile drainage process into the NWM substantially enhanced the accuracy of the NWM over  
 446 heavily tile-drained basins in the upper Midwest.

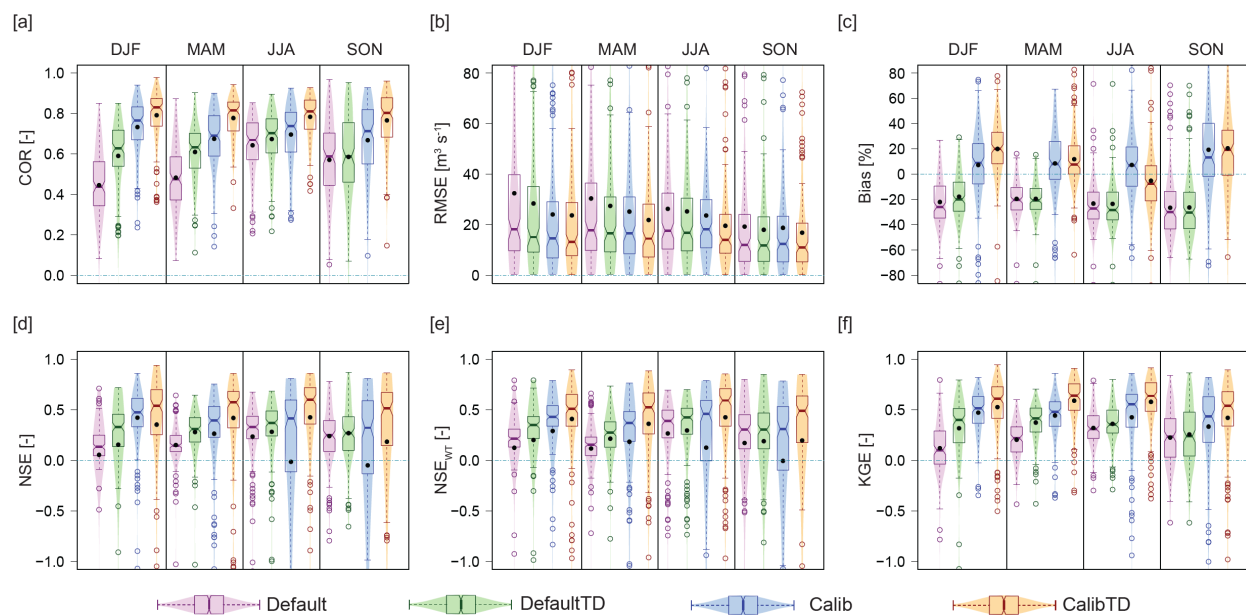


447  
 448 **Figure 3.** The NWM performance evaluation over 49 calibration basins for the calibration and  
 449 validation periods. Comparison of the distribution of six evaluation metrics estimated based on  
 450 the four NWM parameter experiments for the calibration (a-f) and validation (g-l) periods. Here,  
 451 DJF=winter, MAM=spring, JJA=summer and SON=fall. Detailed descriptions of these metrics  
 452 are provided in Table 2.

453

454 **3.3 NWM performance evaluation: Regional Simulation experiments**

455 By employing the regionalized parameters, we conducted the same set of four NWM simulations  
 456 (see section 2.7) to quantify the influence of tile drainage on the NWM performance over the  
 457 heavily tile-drained UMRB and ORB. The distributions of model evaluation metrics estimated  
 458 using 139 USGS streamflow observations are provided in Figure 4. As mentioned earlier,  
 459 *DefaultTD* is able to attain more than 50% of the improvement brought by the fully calibrated  
 460 NWM from *Default* over the regional domain. It substantially enhanced the ability of NWM to  
 461 capture the timing, peaks, and quantity of observed streamflow. The estimated RMSE for the  
 462 *DefaultTD* is 3% to 17% less than that of the *Default*. The improvements we observed in NSE,  
 463  $NSE_{WT}$ , and KGE for the *DefaultTD* are significant ( $p < 0.05$ ) compared to *Default* in all seasons  
 464 except fall (Figure 4 and Table S3). Except for RMSE in all seasons,  $NSE_{WT}$  during summer and  
 465 fall, and NSE during fall, all the model evaluation metrics for the *Calib* showed significant  
 466 improvements from *Default* ( $p < 0.05$ ) (Figure 4 and Table S3).



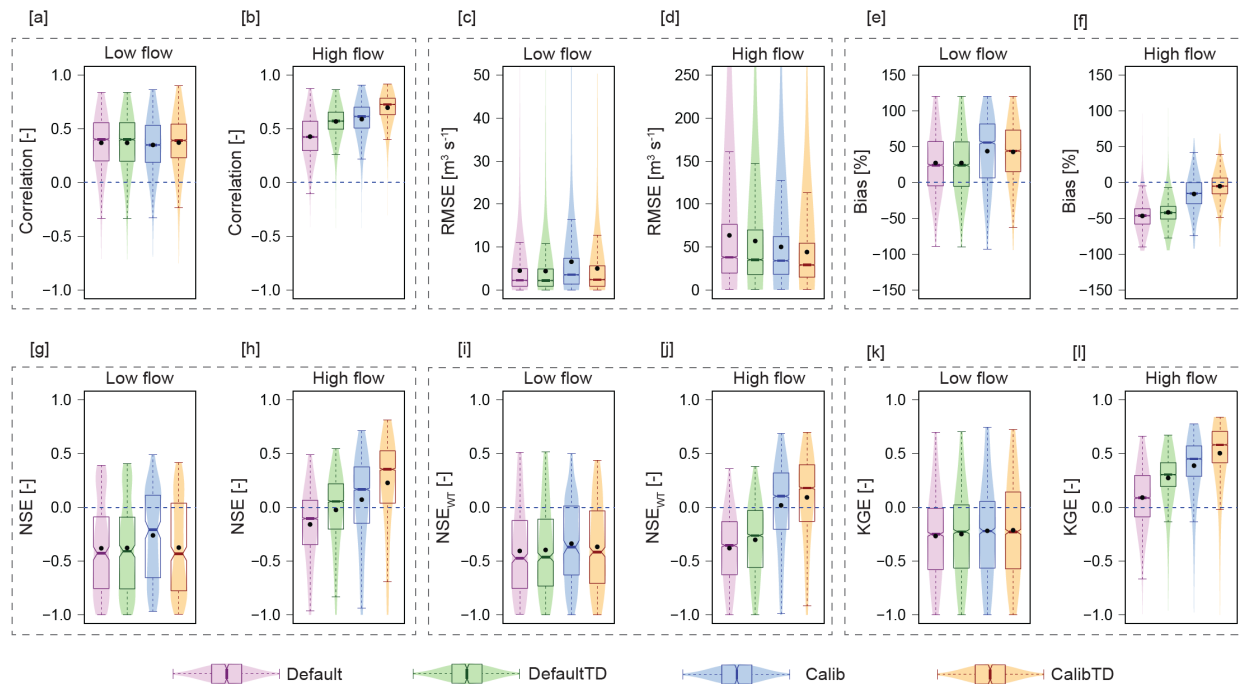
467  
 468 **Figure 4.** Seasonal NWM performance evaluation over the two HUC2 regional domains based  
 469 on 139 USGS streamflow observations. Comparison of the distribution of six evaluation metrics  
 470 estimated based on the four NWM parameter experiments for the regional simulation period (a-  
 471 f). In (a-f), the color shading behind the boxplot indicate the data distribution density.

472

473 One of the main focuses of this study is to quantify the impact of the tile drainage scheme on  
474 calibrated NWM performance over the regional domain, and Figure 4a-f clearly shows a better  
475 performance of the *CalibTD* than *Calib*. Seasonal distributions of the model evaluation metrics  
476 showed significant ( $p < 0.05$ ) improvements in the *CalibTD* performance in reproducing the flow  
477 time, quantity, variance, and dynamics in the observed streamflow than in other model  
478 experiments. RMSE in *CalibTD* is considerably reduced by 9% to 23% compared to *Calib*  
479 (Figure 4b). However, *CalibTD* slightly overestimated (underestimated) streamflow during  
480 winter (summer) compared to observation and *Calib*, but there are no significant differences  
481 between them for spring and fall (Figure 4c and Table S3).

### 482 3.3.1 Hydrograph analysis

483 To understand the causes of discrepancies in the NWM simulated streamflow (mainly Bias and  
484 RMSE), we conducted hydrograph analysis using the NWM simulated streamflow from four  
485 experiments and observations. Results of the high-flow and low-flow hydrograph analysis are  
486 presented in Figure 5. The median values of performance metrics estimated for the low-flows are  
487 almost the same for *Default* and *DefaultTD* (Figure 5a, c, e, g, i, and k). The median low-flow  
488 Bias estimated for *Calib* is twice that of *Default* (Figure 5e). Even though *CalibTD* reduced low-  
489 flow biases compared to *Calib*, it still overestimated low-flows by 50%. Analyzing the  
490 distributions of NSE (Figure 5g), NSE<sub>WT</sub> (Figure 5i), and KGE (Figure 5k) indicated that the  
491 NWM, in general, failed to reproduce observed low-flow accurately, consistent with previous  
492 studies assessing the NWM performance in estimating low-flows have reported similar findings  
493 (Hansen et al., 2019; Jachens et al., 2021; Karki et al., 2021). One of the reasons for the  
494 overestimation of low-flows can be the high groundwater recharge (deep percolation loss) rate in  
495 the NWM (Karki et al., 2021). The existing groundwater scheme in the NWM represents surface  
496 water–groundwater connectivity using a one-way connection from the underlying aquifer to the  
497 stream channel and omitted the influences of the stream on groundwater, and ignoring the two-  
498 way stream–aquifer fluxes in the NWM lead to overprediction of low flows (Jachens et al.,  
499 2021). Our results indicate significant reductions in the low-flow Bias and RMSE in *CalibTD*  
500 compared to *Calib*. Because tile drainage substantially reduced the groundwater recharge and  
501 rerouted the saturated soil water into the stream directly (see section 3.4 for more detailed  
502 discussion).



503

504 **Figure 5.** Evaluation of the NWM simulated high-flows and low-flows based on regional  
 505 simulation. The model performance metrics are calculated by comparing the NWM estimates  
 506 with 139 USGS streamflow observations. In (a-l), the color shading behind the boxplot indicate  
 507 the data distribution density.

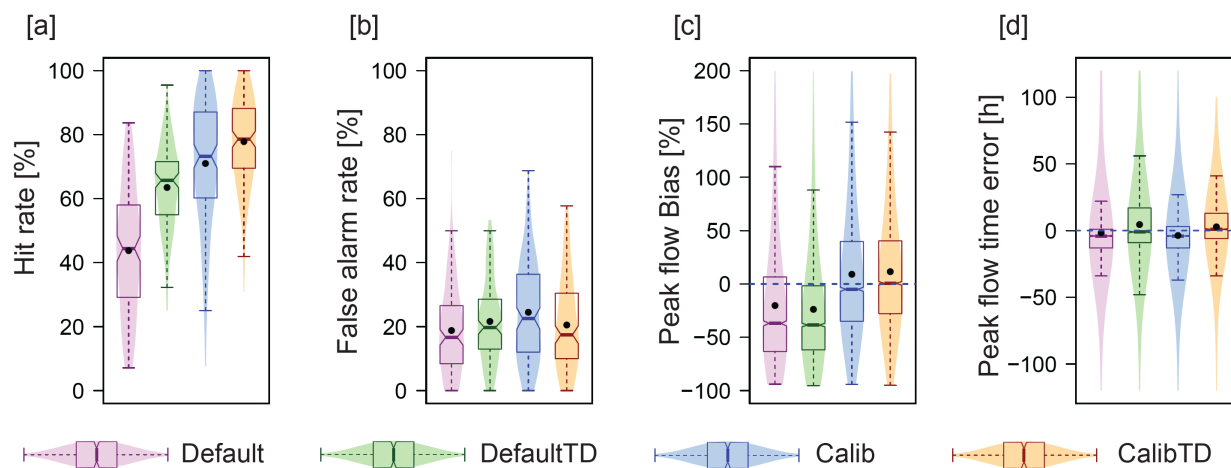
508

509 Results on high-flows revealed considerable improvements in the *DefaultTD* and *CalibTD*  
 510 performance over the regional domain (Figure 5b, d, f, h, j, and l). As we highlighted before,  
 511 *DefaultTD* significantly ( $p < 0.05$ ) improved the high-flow performance of the NWM compared to  
 512 *Default* by increasing COR by 0.15, NSE by 0.16, and KGE by 0.22. Furthermore, *DefaultTD* is  
 513 able to reduce RMSE by  $-2.84 \text{ m}^3 \text{ s}^{-1}$  and improve the Bias by 4.2%. The variability in the model  
 514 performance metrics is considerably lower in *DefaultTD* compared to *Default*. *Calib*  
 515 substantially enhanced performance in reproducing the observed high-flow characteristics than  
 516 *Default*. Analyzing the evaluation metrics of *Calib* indicated a significant ( $p < 0.05$ ) increase in  
 517 COR by 0.19, NSE by 0.27,  $\text{NSE}_{\text{wrt}}$  by 0.46, and KGE by 0.36 than in *Default*. *Calib* can better  
 518 capture the timing and magnitude of observed high-flows with reduced mean error compared to  
 519 *Default*. *CalibTD* further enhanced the accuracy in estimating the observed high-flow  
 520 characteristics by significantly increasing COR by 0.11, NSE by 0.19, and KGE by 0.13 in  
 521 *CalibTD* compared to *Calib* (Figure 5b, h, and l). Furthermore, *CalibTD* reduced the mean error

522 by  $4.88 \text{ m}^3\text{s}^{-1}$  and Bias by 10% (Figure 5d and f). Overall, the NWM with *CalibTD* is able to  
 523 better capture the timing, magnitude, and dynamics of observed high-flows very well compared  
 524 to other experiments.

### 525 3.3.2 Event-based evaluation

526 One important goal of the NWM is to provide flash flood forecasts with longer lead times and  
 527 reduced uncertainties. Thus, we analyzed the performance of NWM to capture the different  
 528 characteristics of observed streamflow events using 139 USGS gage measurements. Event-based  
 529 metrics estimated for different NWM experiments are presented in Figure 6. *Default* is able to  
 530 reproduce about 44% of the observed streamflow events (Figure 6a). The *DefaultTD*  
 531 significantly increased the event hit rate by 47% ( $p < 0.001$ ) than *Default*, and also reduced the  
 532 variability in the hit rate. *Calib* significantly enhanced the hit rate of NWM by 67% ( $p < 0.001$ )  
 533 compared to *Default*. Among the four NWM experiments considered, *CalibTD* showed the  
 534 highest streamflow event hit rate. The estimated hit rate in *CalibTD* is 78%, which is 7% higher  
 535 than *Calib*. Moreover, the spread in the hit rate estimated for *CalibTD* is considerably lower than  
 536 that of *Calib* (Figure 6a). The median false alarm rate in *Calib* is 22.5%. But in *CalibTD*, the  
 537 false alarm rate is substantially reduced to 17.5% (Figure 6b).



538  
 539 **Figure 6.** Event-based evaluation of the NWM based on regional simulation. The event-based  
 540 statistics are calculated by comparing the NWM estimates with 139 USGS streamflow  
 541 observations. In (a-d), the color shading behind the boxplot indicate the data distribution density.

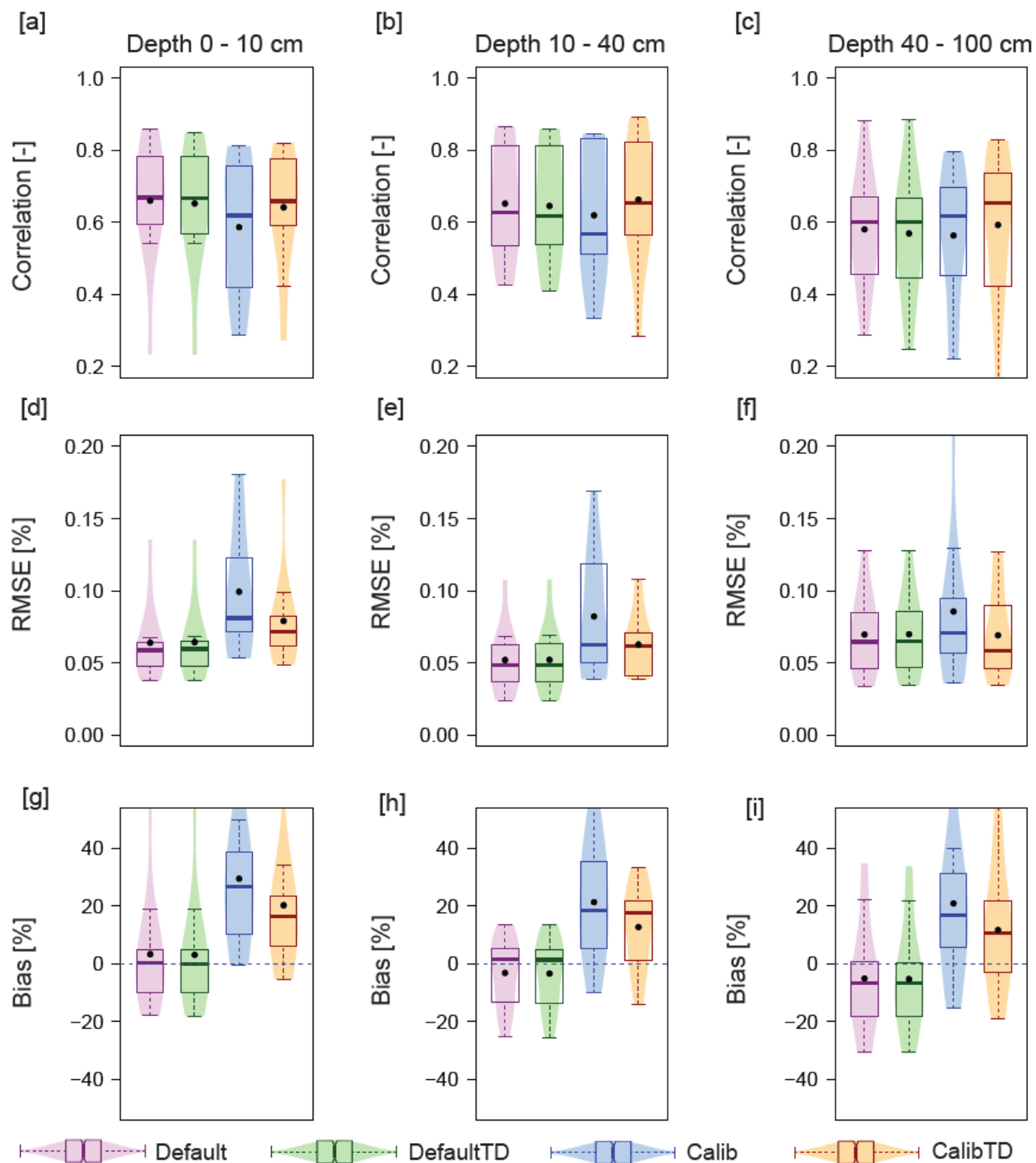
542

543 Tile drainage can significantly impact the peaks and timings of streamflow events, with an  
544 earlier peak of greater magnitude (Rahman et al., 2014; Robinson et al., 1985), so we also  
545 quantified the NWM's ability to capture the peak flows, and timing of peak flows for each  
546 streamflow event. The estimated peak flow bias (%) and peak flow timing error (h) from  
547 different NWM experiments are presented in Figures 6c and 6d, respectively. There is no  
548 considerable difference between *Default* and *DefaultTD* in the estimated peak flow bias.  
549 However, *CalibTD* outperformed *Calib* and produced a lower peak flow bias of 0.57% compared  
550 to 5% in *Calib*. The median values of the estimated peak flow timing error are -3h, 0h, 4h, and  
551 2h for *Default*, *DefaultTD*, *Calib*, and *CalibTD*, respectively. Overall, the event-based  
552 streamflow analysis indicated that NWM with *CalibTD* outperformed other NWM experiments  
553 over the heavily tile-drained UMRB and ORB. Our findings are consistent with previous studies  
554 in that the model performance to simulate streamflow over a heavily tile-drained watershed was  
555 considerably improved when they incorporated tile drainage into the model (Green et al., 2006;  
556 Hansen et al., 2013; Robinson et al., 1985; Wiskow and van der Ploeg, 2003).

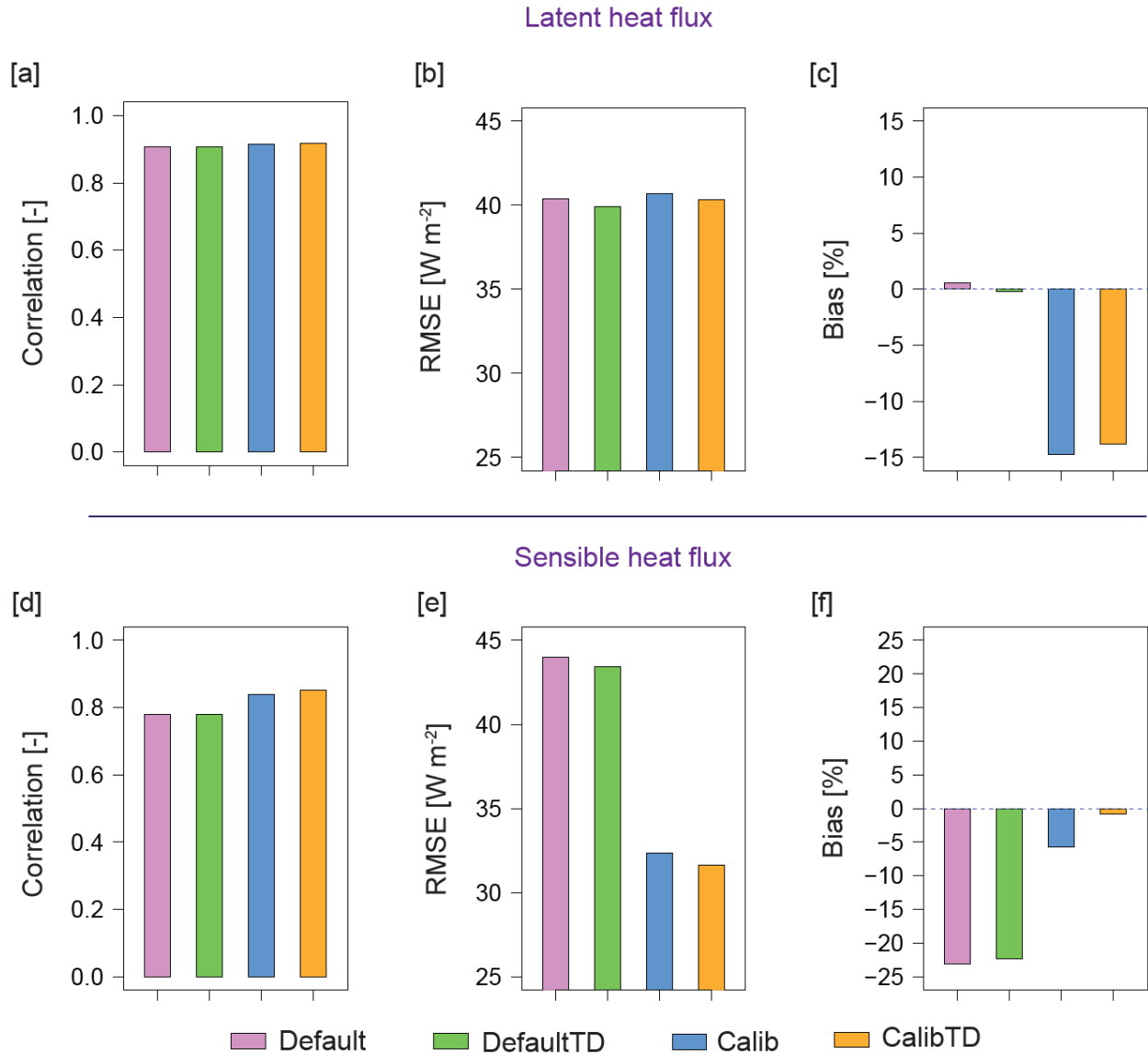
### 557 **3.3.3 Soil moisture evaluation**

558 In addition to streamflow, tile drainage modifies the soil water storage. We evaluated the NWM  
559 performance using soil moisture measurements (volumetric) from 12 sites in the South Fork  
560 Iowa River watershed (Figure 1f). Using the soil moisture measurements from three different  
561 depths and NWM estimates at three model levels, we estimated COR, RMSE, and Bias in the  
562 model estimated soil moisture (Figure 7). The NWM performance in estimating the soil  
563 moisture using *Default* and *DefaultTD* is nearly identical regarding the medians of COR, RMSE.  
564 Both *Default* and *DefaultTD* showed higher median COR (0.68) and zero median Bias for the  
565 first soil layer (0-10 cm) of the NWM. A lower COR (0.60) and Bias (8%) and higher RMSE  
566 (0.062%) are estimated for the third soil layer of the NWM. Calibration substantially impacted  
567 the performance of the NWM to estimate soil moisture. For instance, *Calib* significantly reduced  
568 the NWM performance compared to *Default* by degrading COR, increasing RMSE, Bias, and  
569 their variance. This is not surprising, because the model was calibrated to optimize streamflow  
570 prediction. Although *CalibTD* underperformed compared to *Default* and *DefaultTD*, it produced  
571 better estimates of soil moisture compared to *Calib*. Also, the medians of COR, RMSE, and Bias

572 are significantly improved, and their variances are reduced when NWM employed *CalibTD*  
 573 instead of *Calib*.



574  
 575 **Figure 7.** Evaluation of the NWM simulated soil moisture with field measurements. In (a-i), the  
 576 color shading behind the boxplot indicate the data distribution density.



577

578 **Figure 8.** Accuracy assessment of NWM simulated energy balance components. (a-c) Represent  
 579 the evaluation of NWM simulated latent heat fluxes (evapotranspiration), (d-f) same as (a-c), but  
 580 for sensible heat fluxes.

581

### 582 3.3.4 Energy flux evaluation

583 Using the eddy covariance flux measurements from seven sites in the South Fork Iowa River  
 584 watershed (Figure 1f), we evaluated the NWM simulated hourly sensible heat (SH) fluxes and  
 585 latent heat (LH) fluxes (equivalent to evapotranspiration). Results of the energy flux analysis are  
 586 presented in Figure 8. The results shown in Figure 8 are the averaged values of evaluation

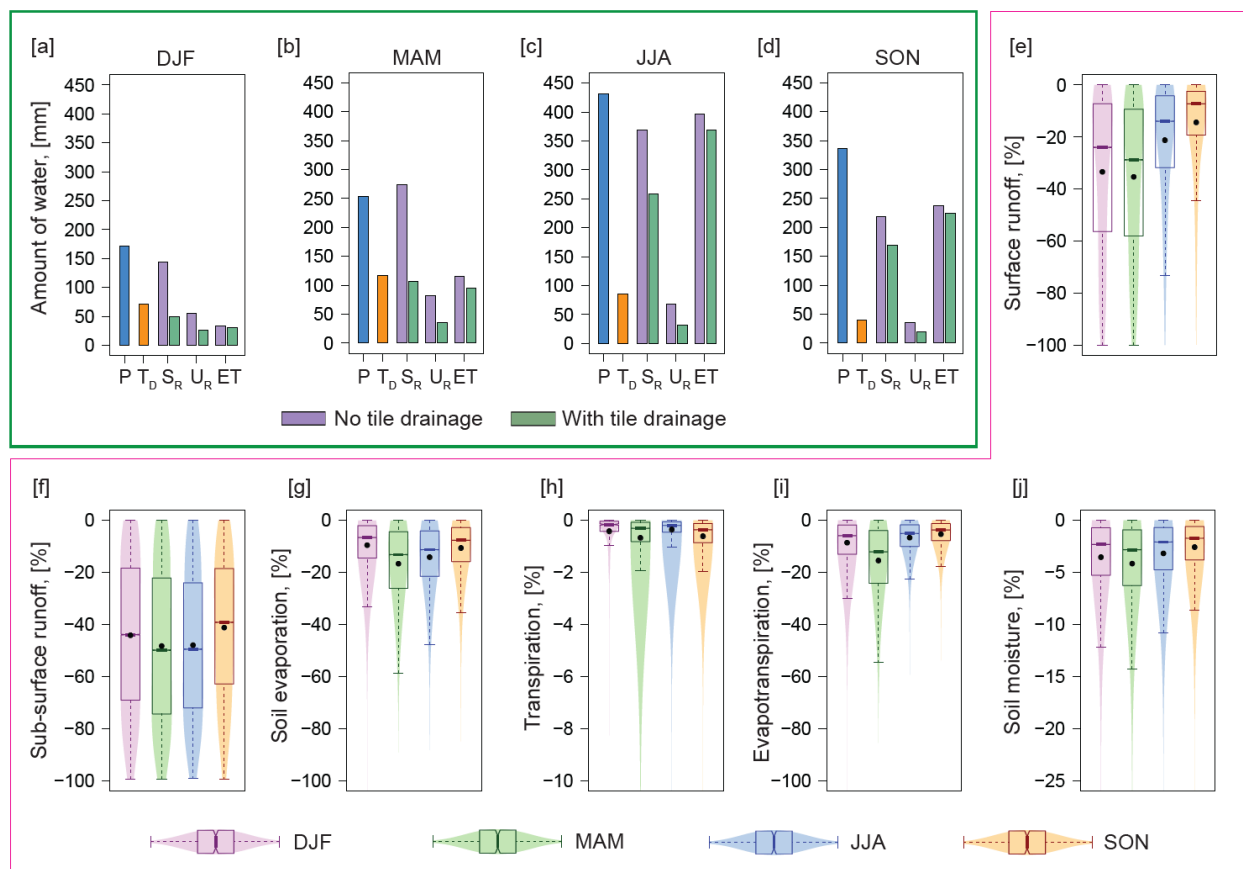
587 metrics estimated for the observation sites. The estimated COR and RMSE of LH for all the four  
588 NWM experiments are almost identical. Despite high correlation, the NWM estimated LH  
589 incurred a high mean error ( $\sim 40 \text{ Wm}^{-2}$ ) (Figure 8b). NWM with *Default* and *DefaultTD*  
590 produced better estimates of LH with Bias equal to  $\pm 1\%$ . However, *Calib* and *CalibTD*  
591 noticeably underestimated LH by -15% and -14%, respectively. In the case of SH, *CalibTD*  
592 outperforms other NWM experiments with higher COR (0.83) and lower RMSE ( $32 \text{ W m}^{-2}$ ) and  
593 Bias (1%). *Calib* considerably enhanced the NWM performance in SH estimation compared to  
594 *Default* and *DefaultTD*. However, *Calib* slightly underperformed compared to *CalibTD*. Even  
595 though there are discrepancies in the NWM estimated SH and LH, our results of LH and SH  
596 indicate that the performance of the NWM is acceptable (see Table 2 for metrics ranges).

### 597 **3.4. Effect of tile drainage on regional hydrology**

598 To quantify the effects of tile drainage on regional hydrology, we analyzed land surface water  
599 balance. For this purpose, we conducted one additional NWM simulation with *CalibTD*  
600 parameters and deactivated the tile drainage scheme. This simulation with a deactivated tile  
601 drainage scheme is designated as “No tile drainage,” (which is not equal to *Calib* as it uses  
602 *CalibTD* parameter set) and the NWM with *CalibTD* is defined as “With tile drainage” in this  
603 section. The results of the seasonal water balance analysis are presented in Figure 9. The results  
604 shown in Figure 9a-d are the averaged values of water balance components estimated for the tile-  
605 drained grids of the NWM within UMRB and ORB. The maximum amount of tile drainage over  
606 UMRB and ORB occurred during spring ( $117 \pm 50 \text{ mm}$ ) followed by summer ( $85 \pm 32 \text{ mm}$ ),  
607 winter ( $71 \pm 40 \text{ mm}$ ), and fall ( $40 \pm 20 \text{ mm}$ ) (Figure 9a-d). Values in the parenthesis indicate  
608 mean and one spatial standard deviation. The ratio of tile-drained water ( $T_D$ ) to precipitation ( $P$ )  
609 is highest during spring (0.46), followed by winter (0.41), summer (0.20), and fall (0.12).

610 The results shown in Figure 9e-j are the distributions of percentage changes in the average values  
611 of water balance components that are calculated for each tile-drained grid of the NWM within  
612 UMRB and ORB. Analyzing seasonal distributions of surface runoff ( $S_R$ ) changes indicated a  
613 significant decrease in  $S_R$  due to tile drainage (Figure 9e), which is consistent with previous  
614 studies (Natho-Jina et al., 1987; Robinson et al., 1985; Robinson and Rycroft, 1999; Skaggs et  
615 al., 1994). Following the seasonal tile drainage pattern, the highest decline in  $S_R$  is estimated for  
616 spring (-29%), followed by winter (-24%), summer (-14%), and fall (-7%). Tile drainage

617 significantly decreased subsurface runoff or groundwater recharge ( $U_R$ ) for all the seasons we  
 618 considered (Figure 9f). This is similar to the findings of Golmohammadi et al. (2017). However,  
 619 a maximum decrease is identified during spring (-50%) and summer (-50%). During winter and  
 620 fall,  $U_R$  decreased by -43% and -39%, respectively. The impact of tile drainage on  $S_R$  is higher  
 621 than  $U_R$  because tile drainage increases infiltration. However, all the saturation water from the  
 622 infiltration are not removed by the tile drainage and a considerable amount of saturation water  
 623 (5% to 10%) is still available to  $U_R$ .



624  
 625 **Figure 9.** Impact of tile drainage on the NWM water balance components. (a-d) The seasonal  
 626 totals of precipitation (P), tile drainage ( $T_D$ ), surface runoff ( $S_R$ ), underground runoff or  
 627 groundwater recharge ( $U_R$ ), and evapotranspiration (ET). The values represented in (a-d) are the  
 628 averages of all the NWM tile-drained grids in the UMRB and ORB. (e-j) The changes in water  
 629 balance components due to tile drainage. The results presented in (e-j), are estimated as “with tile  
 630 drainage” minus “no tile drainage”. In (e-j), the color shading behind the boxplot indicate the  
 631 distribution density.

632 The main components of evapotranspiration (ET) are direct soil evaporation, transpiration, and  
633 canopy evaporation. Our analysis indicated that tile drainage significantly impacted soil  
634 evaporation (Figure 9g). The seasonal distributions of soil evaporation changes showed a more  
635 significant decrease in spring (-13%) and summer (-11%) ( $p < 0.05$ ). The reduction in soil  
636 evaporation estimated for winter and fall are -7% and -8%, respectively. Since the results on  
637 transpiration indicated minimal changes ( $< 1\%$ ) due to tile drainage, the estimated seasonal  
638 changes in ET are almost equal to soil evaporation (Figure 9i). Studies of Khand et al. (2017),  
639 Kjaersgaard et al. (2014), and Yang et al. (2017) based on remote sensing and eddy covariance  
640 ET measurements from tile-drained croplands of the US reported similar findings on ET  
641 changes. Furthermore, we also evaluated the impact of tile drainage on root-zone soil moisture.  
642 Our results indicate that the soil moisture considerably decreased by 2% to 3% due to tile  
643 drainage. Similar findings were previously reported by many studies (Fausey 2005; Fraser and  
644 Flemming, 2001; King et al., 2014).

645 Additionally, we quantified the impact of tile drainage on streamflow by comparing “No tile  
646 drainage” with “With tile drainage”. Tile drainage substantially altered the streamflow events by  
647 increasing peaks by 14%, increasing volume by 2.3%, delaying event start time by 2 hours, and  
648 reducing the end time by 7 hours. As indicated by previous studies, tile drainage is responsible  
649 for more short-term flashy streamflow events (De Schepper, 2017; Miller and Lyon, 2021;  
650 Rahman et al., 2014; Robinson et al., 1985). Our results indicated a considerable increase in  
651 seasonal streamflow volume due to tile drainage. The highest increase is estimated for winter  
652 (17%), followed by spring (13%), fall (13%), and summer (2.8%). Moreover, our analysis found  
653 that tile drainage enhanced the baseflow volume by 11.52%, which consistent with findings from  
654 previous studies (King et al., 2014; Moore and Larson, 1980; Schilling and Libra, 2003).  
655 However, the baseflow index is estimated as the ratio of total baseflow to the total streamflow is  
656 decreased by -9.10%. In other words, the impact of tile drainage on direct runoff (or quick flow)  
657 is more substantial compared to baseflow (Miller and Lyon, 2021). Overall, tile drainage has  
658 significant effects on most of the water balance components in the study domain.

#### 659 **4. Conclusion**

660 The purpose of the study is to quantify the impacts of representing subsurface tile drainage on  
661 the National Water Model’s simulated regional hydrology. We implemented Hooghoudt’s tile

662 drainage scheme into the NWM V2.0 and used 30-m resolution AgTile-US to identify tile-  
663 drained grids within the model domain. We followed the operational NWM calibration approach  
664 and calibrated 14 sensitive NWM parameters (Dugger et al., 2017; Gochis et al., 2019) along  
665 with tile spacing. Overall, the changes in these parameters suggested a water-absorbing soil  
666 column with higher infiltration rates and moisture storage potential. The calibration results also  
667 indicated reduced surface runoff and evapotranspiration over the tile-drained croplands.

668 Representing the tile drainage process in the NWM significantly improved its performance in  
669 estimating streamflow over the UMRB and ORB. More interestingly, the NWM with  
670 uncalibrated parameters but including a tile drainage scheme (i.e., *DefaultTD*) attained 20% to  
671 50% of the improvements brought by the calibrated NWM (*Calib*) from *Default*. The *CalibTD*  
672 outperformed other experiments with reduced RMSE, Bias, and increased NSE, COR, and KGE.  
673 Furthermore, *CalibTD* accurately captured the dynamics in magnitude, timing, and variability of  
674 observed streamflow, especially the high-flows and low-flows. Tile drainage substantially  
675 increased peak flows, baseflow, and event volume. This significantly enhanced accuracy of the  
676 NWM to simulate high-flows in *CalibTD*. Even though *CalibTD* produced better estimates of  
677 low-flows than *Calib*, there is considerable uncertainty in the estimated low-flow timings and  
678 magnitudes. The overestimation of low-flows by the NWM can be caused by high groundwater  
679 recharge rates or lack of realism in the groundwater scheme in the NWM. Despite these  
680 discrepancies, NWM with a tile drainage scheme better estimates soil moisture, latent heat fluxes  
681 (or evapotranspiration), and sensible heat fluxes for the tile-drained croplands.

682 We quantified the impact of tile drainage on different water balance components, and our results  
683 indicated a significant decrease in the surface runoff, underground runoff or groundwater  
684 recharge, and evapotranspiration over UMRB and ORB. The impact of tile drainage on direct  
685 runoff (or quick flow) is more profound than on baseflow. The drainage of saturated water from  
686 the soil column by the subsurface tiles reduced the deep percolation of free water into the  
687 groundwater reservoir (Golmohammadi et al., 2017). Tile drainage removed saturated water  
688 from the soil column above the tiles and increased soil storage potential (Rahman et al., 2014).  
689 The decrease in ET over the tile drained croplands is mainly due to reduced direct soil  
690 evaporation resulting from low soil water content (Moriassi et al., 2012; Rahman et al., 2014).

691 Overall, tile drainage has a significant impact on regional hydrology. The representation of tile  
692 drainage process in the NWM can enhance the model's accuracy to estimate the dynamics of  
693 streamflow mainly, the timing, peaks, and volume of streamflow over a heavily tile-drained  
694 basin. Thus, our findings demonstrate the importance of incorporating tile drainage into the  
695 operational NWM for accurate flood forecasts.

#### 696 **Data and Code Availability Statement**

697 All data used to generate the major figures are publicly available. The AORC data are accessed  
698 from <https://hydrology.nws.noaa.gov/pub/aorc-historic/>. The USGS streamflow data are  
699 available at: <https://waterdata.usgs.gov/nwis/inventory/>. The NLCD land cover data are available  
700 at: <https://www.mrlc.gov/data/>. The AgTile-US 30-m tile drainage map is available at:  
701 <https://figshare.com/articles/dataset/AgTile-US/11825742/>. NHDPlusV2 data can be accessed  
702 from [https://nhdplus.com/NHDPlus/NHDPlusV2\\_data.php](https://nhdplus.com/NHDPlus/NHDPlusV2_data.php). The South Fork Iowa River  
703 watershed soil moisture and flux data are obtained from Coopersmith et al. (2015; 2021)  
704 (<https://hrsl.ba.ars.usda.gov/southfork/index.html>). The NWM source code used in this study is  
705 publicly available at: [https://github.com/NCAR/wrf\\_hydro\\_nwm\\_public/](https://github.com/NCAR/wrf_hydro_nwm_public/). The RNWMStat R-  
706 Package is available at: <https://github.com/NCAR/RNWMStat/>.

#### 707 **Acknowledgements**

708 We would like to acknowledge the support from the NOAA OAR grant NA18OAR4590381,  
709 NCAR Water System, USDA NIFA grants 2015-67003-23508 and 2015-67003-23460, and the  
710 NSF INFEWS grant 1739705. We would like to acknowledge Dr. Brian Cosgrove, Office of  
711 Water Prediction, NOAA/NWS, Silver Spring, MD, for his unconditional support in various  
712 stages of this work. Simulations are conducted using computing resources from Cheyenne High  
713 Performance Computing (<https://doi.org/10.5065/D6RX99HX>) provided by NCAR's  
714 Computational and Information Systems Laboratory, sponsored by the NSF. We are grateful to  
715 three anonymous reviewers for their valuable comments.

716 **References**

- 717 Arnold, J. G., Srinivasan, R., Muttiah, R. S., & Allen, P. M. (1999). Continental scale simulation  
718 of the hydrologic balance. *JAWRA Journal of the American Water Resources*  
719 *Association*, 35(5), 1037-1051. <https://doi.org/10.1111/j.1752-1688.1999.tb04192.x>
- 720 Barlage, M., Chen, F., Rasmussen, R., Zhang, Z., & Miguez-Macho, G. (2021). The Importance  
721 of Scale-Dependent Groundwater Processes in Land-Atmosphere Interactions Over the  
722 Central United States. *Geophysical Research Letters*, 48(5), e2020GL092171.  
723 <https://doi.org/10.1029/2020GL092171>
- 724 Beck, H.E., van Dijk, A.I., De Roo, A., Miralles, D.G., McVicar, T.R., Schellekens, J., &  
725 Bruijnzeel, L.A. (2016). Global-scale regionalization of hydrologic model parameters. *Water*  
726 *Resources Research*, 52(5), pp.3599-3622. <https://doi.org/10.1002/2015WR018247>
- 727 Benesty, J., Chen, J., Huang, Y., & Cohen, I. (2009). Pearson correlation coefficient. In *Noise*  
728 *reduction in speech processing* (pp. 1-4). Springer, Berlin, Heidelberg.  
729 [https://doi.org/10.1007/978-3-642-00296-0\\_5](https://doi.org/10.1007/978-3-642-00296-0_5)
- 730 Blann, K. L., Anderson, J. L., Sands, G. R., & Vondracek, B. (2009). Effects of agricultural  
731 drainage on aquatic ecosystems: a review. *Critical reviews in environmental science and*  
732 *technology*, 39(11), 909-1001. <https://doi.org/10.1080/10643380801977966>
- 733 Clapp, R.B., & Hornberger, G.M. (1978). Empirical equations for some soil hydraulic properties.  
734 *Water resources research*, 14(4), pp.601-604. <https://doi.org/10.1029/WR014i004p00601>
- 735 Coopersmith, E.J., Cosh, M.H., Petersen, W.A., Prueger, J., & Niemeier, J.J. (2015). Soil  
736 moisture model calibration and validation: An ARS watershed on the South Fork Iowa  
737 River. *Journal of Hydrometeorology*, 16(3), pp.1087-1101. [https://doi.org/10.1175/JHM-D-](https://doi.org/10.1175/JHM-D-14-0145.1)  
738 [14-0145.1](https://doi.org/10.1175/JHM-D-14-0145.1)
- 739 Coopersmith, E.J., Cosh, M.H., Starks, P.J., Bosch, D.D., Holifield Collins, C., Seyfried, M.,  
740 Livingston, S., & Prueger, J. (2021). Understanding temporal stability: a long-term analysis of  
741 USDA ARS watersheds. *International Journal of Digital Earth*, pp.1-12.  
742 <https://doi.org/10.1080/17538947.2021.1943550>

743 Daly, C., Gibson, W.P., Taylor, G.H., Johnson, G.L., & Pasteris, P. (2002). A knowledge-based  
744 approach to the statistical mapping of climate. *Climate research*, 22(2), pp.99-113.  
745 <http://dx.doi.org/10.3354/cr022099>

746 De Schepper, G., Therrien, R., Refsgaard, J. C., He, X., Kjaergaard, C., & Iversen, B. V. (2017).  
747 Simulating seasonal variations of tile drainage discharge in an agricultural catchment. *Water*  
748 *Resources Research*, 53(5), 3896-3920. <https://doi.org/10.1002/2016WR020209>

749 Du, B., Arnold, J. G., Saleh, A., & Jaynes, D. B. (2005). Development and application of SWAT  
750 to landscapes with tiles and potholes. *Transactions of the ASAE*, 48(3), 1121-1133.  
751 <http://dx.doi.org/10.13031/2013.18522>

752 Dugger, A. L., Gochis, D. J., Yu, W., Barlage, M., Yang, Y., McCreight, J., Karsten, L.,  
753 Rafieeinassab, A., & Sampson, K. (2017). Learning from the National WaterModel: Regional  
754 improvements in streamflow prediction through experimental parameter and physics updates  
755 to the WRF-Hydro Community Model. 31st Conf. on Hydrology, Seattle, WA, Amer.Meteor.  
756 Soc.,6A.3.

757 Eastman, M., Gollamudi, A., Stämpfli, N., Madramootoo, C. A., & Sarangi, A. (2010).  
758 Comparative evaluation of phosphorus losses from subsurface and naturally drained  
759 agricultural fields in the Pike River watershed of Quebec, Canada. *Agricultural Water*  
760 *Management*, 97(5), 596-604. <http://dx.doi.org/10.1016/j.agwat.2009.11.010>

761 Fausey, N. R. (2005). Drainage management for humid regions. *International Agricultural*  
762 *Engineering Journal*, 14(4), 209-214.

763 Fausey, N. R., Doering, E. J., Palmer, M. L., & Pavelis, G. A. (1987). Purposes and benefits of  
764 drainage. *Economic Research Service, US Department of Agriculture: Washington, 1455*, 48-  
765 51.

766 Feddema, J. J. (2005). A revised Thornthwaite-type global climate classification. *Physical*  
767 *Geography*, 26(6), 442-466. <https://doi.org/10.2747/0272-3646.26.6.442>

768 Feng, X., Rafieeinassab, A., Karsten, L., Wu, W., Kitzmiller, D., Liu, Y., Cosgrove, B., Read, L.,  
769 Dugger, A.L., Zhang, Y., & FitzGerald, K. (2019). Calibrating the National Water Model V2.

770 1 over the Contiguous United States. In *AGU Fall Meeting Abstracts* (Vol. 2019, pp. H43I-  
771 2134).

772 Fraser, H., Fleming, R., & Eng, P. (2001). Environmental benefits of tile drainage. *Prepared for:*  
773 *LICO. Land Improvement Contractors of Ontario. Ridgetown College, University of Guelph.*

774 Garambois, P.A., Roux, H., Larnier, K., Labat, D., & Dartus, D. (2015). Parameter  
775 regionalization for a process-oriented distributed model dedicated to flash floods. *Journal of*  
776 *Hydrology*, 525, pp.383-399. <https://doi.org/10.1016/j.jhydrol.2015.03.052>

777 Gharari, S., Hrachowitz, M., Fenicia, F., Gao, H., & Savenije, H.H.G. (2014). Using expert  
778 knowledge to increase realism in environmental system models can dramatically reduce the  
779 need for calibration. *Hydrology and Earth System Sciences*, 18(12), pp.4839-4859.  
780 <https://doi.org/10.5194/hess-18-4839-2014>

781 Gochis, D., Yates, D., Sampson, K., Dugger, A., McCreight, J., Barlage, M., RafieeiNasab, A.,  
782 Karsten, L., Read, L., Zhang, Y., & McAllister, M. (2019). Overview of national water model  
783 calibration general strategy & optimization. *National Center for Atmospheric Research.*

784 Gochis, D.J., Barlage, M., Dugger, A., FitzGerald, K., Karsten, L., McAllister, M., McCreight,  
785 J., Mills, J., RafieeiNasab, A., Read, L., Sampson, K., Yates, D., & Yu, W. (2018). The WRF-  
786 Hydro modeling system technical description, (Version 5.0). NCAR Technical Note. 107  
787 pages. Available online at:  
788 <https://ral.ucar.edu/sites/default/files/public/WRFHydroV5TechnicalDescription.pdf>.

789 Golmohammadi, G., Rudra, R., Prasher, S., Madani, A., Youssef, M., Goel, P., & Mohammadi,  
790 K. (2017). Impact of tile drainage on water budget and spatial distribution of sediment  
791 generating areas in an agricultural watershed. *Agricultural Water Management*, 184, 124-134.  
792 <http://dx.doi.org/10.1016/j.agwat.2017.02.001>

793 Gower, J.C. (1971). A general coefficient of similarity and some of its properties. *Biometrics*,  
794 pp.857-871. <https://doi.org/10.2307/2528823>

795 Green, C. H., Tomer, M. D., Di Luzio, M., & Arnold, J. G. (2006). Hydrologic evaluation of the  
796 soil and water assessment tool for a large tile-drained watershed in Iowa. *Transactions of the*  
797 *ASABE*, 49(2), 413-422. <https://doi.org/10.13031/2013.20415>

798 Guanter, L., Zhang, Y., Jung, M., Joiner, J., Voigt, M., Berry, J.A., Frankenberg, C., Huete,  
799 A.R., Zarco-Tejada, P., Lee, J.E., & Moran, M.S. (2014). Global and time-resolved  
800 monitoring of crop photosynthesis with chlorophyll fluorescence. *Proceedings of the National*  
801 *Academy of Sciences*, 111(14), pp.E1327-E1333. <https://doi.org/10.1073/pnas.1320008111>

802 Guo, T., Gitau, M., Merwade, V., Arnold, J., Srinivasan, R., Hirschi, M., & Engel, B. (2018).  
803 Comparison of performance of tile drainage routines in SWAT 2009 and 2012 in an  
804 extensively tile-drained watershed in the Midwest. *Hydrology and Earth System*  
805 *Sciences*, 22(1), 89-110. <https://doi.org/10.5194/hess-22-89-2018>

806 Gupta, H. V., Kling, H., Yilmaz, K. K., & Martinez, G. F. (2009). Decomposition of the mean  
807 squared error and NSE performance criteria: Implications for improving hydrological  
808 modelling. *Journal of hydrology*, 377(1-2), 80-91.  
809 <https://doi.org/10.1016/J.JHYDROL.2009.08.003>

810 Gupta, H.V., Sorooshian, S., & Yapo, P.O. (1998). Toward improved calibration of hydrologic  
811 models: Multiple and noncommensurable measures of information. *Water Resources*  
812 *Research*, 34(4), pp.751-763. <https://doi.org/10.1029/97WR03495>

813 Hansen, A. L., Refsgaard, J. C., Christensen, B. S. B., & Jensen, K. H. (2013). Importance of  
814 including small-scale tile drain discharge in the calibration of a coupled groundwater-surface  
815 water catchment model. *Water Resources Research*, 49(1), 585-603.  
816 <http://dx.doi.org/10.1029/2011WR011783>

817 He, Y., Bárdossy, A., & Zehe, E. (2011). A review of regionalisation for continuous streamflow  
818 simulation. *Hydrology and Earth System Sciences*, 15(11), pp.3539-3553.  
819 <https://doi.org/10.5194/hess-15-3539-2011>

820 Hooghoudt, S. B. (1940). General consideration of the problem of field drainage by parallel  
821 drains, ditches, watercourses, and channels. *Contribution to the knowledge of some physical*  
822 *parameters of the soil*, 7.

823 Hrachowitz, M., Savenije, H.H.G., Blöschl, G., McDonnell, J.J., Sivapalan, M., Pomeroy, J.W.,  
824 Arheimer, B., Blume, T., Clark, M.P., Ehret, U., & Fenicia, F. (2013). A decade of Predictions

825 in Ungauged Basins. *Hydrolog. Sci. J.*, p.803183.  
826 <https://doi.org/10.1080/02626667.2013.803183>

827 Huffman, R. L., Fangmeier, D. D., Elliot, W. J., Workman, S. R., & Schwab, G. O. (2011). *Soil*  
828 *and water conservation engineering*. St. Joseph: American Society of Agricultural and  
829 Biological Engineers. <https://doi.org/10.13031/swce.2013>

830 Jachens, E. R., Hutcheson, H., Thomas, M. B., & Steward, D. R. (2021). Effects of  
831 Groundwater-Surface Water Exchange Mechanism in the National Water Model over the  
832 Northern High Plains Aquifer, USA. *JAWRA Journal of the American Water Resources*  
833 *Association*, 57(2), 241-255. <https://doi.org/10.1111/1752-1688.12869>

834 Joyce, R.J., Janowiak, J.E., Arkin, P.A., & Xie, P. (2004). CMORPH: A method that produces  
835 global precipitation estimates from passive microwave and infrared data at high spatial and  
836 temporal resolution. *Journal of hydrometeorology*, 5(3), pp.487-503.  
837 [https://doi.org/10.1175/1525-7541\(2004\)005<0487:CAMTPG>2.0.CO;2](https://doi.org/10.1175/1525-7541(2004)005<0487:CAMTPG>2.0.CO;2)

838 Julien, P. Y., Saghafian, B., & Ogden, F. L. (1995). Raster-based hydrologic modeling of  
839 spatially-varied surface runoff. *JAWRA Journal of the American Water Resources*  
840 *Association*, 31(3), 523-536. <https://doi.org/10.1111/j.1752-1688.1995.tb04039.x>

841 Kalita, P.K., Cooke, R.A., Anderson, S.M., Hirschi, M.C., & Mitchell, J.K. (2007). Subsurface  
842 drainage and water quality: The Illinois experience. *Transactions of the ASABE*, 50(5),  
843 pp.1651-1656. <https://doi.org/10.13031/2013.23963>

844 Karki, R., Krienert, J.M., Hong, M., & Steward, D.R. (2021). Evaluating Baseflow Simulation in  
845 the National Water Model: A Case Study in the Northern High Plains Region, USA. *JAWRA*  
846 *Journal of the American Water Resources Association*, 57(2), pp.267-280.  
847 <https://doi.org/10.1111/1752-1688.12911>

848 Khand, K., Kjaersgaard, J., Hay, C., & Jia, X. (2017). Estimating impacts of agricultural  
849 subsurface drainage on evapotranspiration using the Landsat imagery-based METRIC  
850 model. *Hydrology*, 4(4), 49. <https://doi.org/10.3390/hydrology4040049>

- 851 King, K. W., Fausey, N. R., & Williams, M. R. (2014). Effect of subsurface drainage on  
852 streamflow in an agricultural headwater watershed. *Journal of hydrology*, 519, 438-445.  
853 <https://doi.org/10.1016/j.jhydrol.2014.07.035>
- 854 Kitze, D.H., Wu, W., Zhang, Z., Patrick, N., & Tan, X. (2018). The Analysis of Record for  
855 Calibration: A High-Resolution Precipitation and Surface Weather Dataset for the United  
856 States. In *AGU Fall Meeting Abstracts* (Vol. 2018, pp. H41H-06).  
857 <https://ui.adsabs.harvard.edu/#abs/2018AGUFM.H41H..06K/abstract>
- 858 Kjaersgaard, J., Khand, K., Hay, C., & Jia, X. (2014). Estimating Evapotranspiration from Fields  
859 with and without Tile Drainage Using Remote Sensing. In *World Environmental and Water  
860 Resources Congress 2014* (pp. 1745-1753).
- 861 Knoben, W. J., Freer, J. E., & Woods, R. A. (2019). Inherent benchmark or not? Comparing  
862 Nash–Sutcliffe and Kling–Gupta efficiency scores. *Hydrology and Earth System Sciences*,  
863 23(10), 4323-4331. <https://doi.org/10.5194/hess-23-4323-2019>
- 864 Kornecki, T. S., & Fouss, J. L. (2001). Quantifying soil trafficability improvements provided by  
865 subsurface drainage for field crop operations in Louisiana. *Applied Engineering in  
866 Agriculture*, 17(6), 777. <http://dx.doi.org/10.13031/2013.6846>
- 867 Leibowitz, S. G., Comeleo, R. L., Wigington Jr, P. J., Weber, M. H., Sproles, E. A., & Sawicz,  
868 K. A. (2016). Hydrologic landscape characterization for the Pacific Northwest, USA. *JAWRA  
869 Journal of the American Water Resources Association*, 52(2), 473-493.  
870 <https://doi.org/10.1111/1752-1688.12402>
- 871 Lin, Y. & Mitchell, K.E. (2005). 1.2 the NCEP stage II/IV hourly precipitation analyses:  
872 Development and applications. In *Proceedings of the 19th Conference Hydrology, American  
873 Meteorological Society, San Diego, CA, USA* (Vol. 10).
- 874 Lipiec, J., Kuś, J., Słowińska-Jurkiewicz, A., & Nosalewicz, A. (2006). Soil porosity and water  
875 infiltration as influenced by tillage methods. *Soil and Tillage research*, 89(2), pp.210-220.  
876 <https://doi.org/10.1016/j.still.2005.07.012>

877 Liu, Y.Q., Durcik, M., Gupta, H.V., & Wagener, T. (2008). Developing distributed conceptual  
878 hydrological models from geospatial databases. *Groundwater-surface water interaction:  
879 process understanding, conceptualization and modelling*, pp.94-102.

880 Livneh, B., Kumar, R., & Samaniego, L. (2015). Influence of soil textural properties on  
881 hydrologic fluxes in the Mississippi river basin. *Hydrological Processes*, 29(21), pp.4638-  
882 4655. <https://doi.org/10.1002/hyp.10601>

883 Livneh, B., Rosenberg, E.A., Lin, C., Nijssen, B., Mishra, V., Andreadis, K.M., Maurer, E.P., &  
884 Lettenmaier, D.P. (2013). A long-term hydrologically based dataset of land surface fluxes and  
885 states for the conterminous United States: Update and extensions. *Journal of Climate*, 26(23),  
886 pp.9384-9392. <http://dx.doi.org/10.1175/JCLI-D-12-00508.s1>

887 Ljung, L. (1999). System identification: theory for the user. *PTR Prentice Hall, Upper Saddle  
888 River, NJ*, 28.

889 Ma, L., Malone, R.W., Heilman, P., Ahuja, L.R., Meade, T., Saseendran, S.A., Ascough II, J.C.,  
890 & Kanwar, R.S. (2007). Sensitivity of tile drainage flow and crop yield on measured and  
891 calibrated soil hydraulic properties. *Geoderma*, 140(3), pp.284-296.  
892 <http://dx.doi.org/10.1016/j.geoderma.2007.04.012>

893 Magner, J. A., Payne, G. A., & Steffen, L. J. (2004). Drainage effects on stream nitrate-N and  
894 hydrology in south-central Minnesota (USA). *Environmental monitoring and  
895 assessment*, 91(1), 183-198. <https://doi.org/10.1023/B:EMAS.0000009235.50413.42>

896 Mallakpour, I., & Villarini, G. (2015). The changing nature of flooding across the central United  
897 States. *Nature Climate Change*, 5(3), 250-254. <https://doi.org/10.1038/nclimate2516>

898 Miller, D.A., & White, R.A. (1998). A conterminous United States multilayer soil characteristics  
899 dataset for regional climate and hydrology modeling. *Earth interactions*, 2(2), pp.1-26.  
900 [https://doi.org/10.1175/1087-3562\(1998\)002%3C0001:ACUSMS%3E2.3.CO;2](https://doi.org/10.1175/1087-3562(1998)002%3C0001:ACUSMS%3E2.3.CO;2)

901 Miller, S. A., & Lyon, S. W. (2021). Tile drainage causes flashy streamflow response in Ohio  
902 watersheds. *Hydrological Processes*, 35(8), e14326. <https://doi.org/10.1002/hyp.14326>

- 903 Moody, W. T. (1967). Closure to “Nonlinear Differential Equation of Drain Spacing”. *Journal of*  
904 *the Irrigation and Drainage Division*, 93(3), 265-269.  
905 <https://doi.org/10.1061/JRCEA4.0000511>
- 906 Moore, I. D., & Larson, C. L. (1980). Hydrologic impact of draining small depressional  
907 watersheds. *Journal of the Irrigation and Drainage Division*, 106(4), 345-363.  
908 <https://doi.org/10.1061/JRCEA4.0001324>
- 909 Moriasi, D. N., Arnold, J. G., Van Liew, M. W., Bingner, R. L., Harmel, R. D., & Veith, T. L.  
910 (2007). Model evaluation guidelines for systematic quantification of accuracy in watershed  
911 simulations. *Transactions of the ASABE*, 50(3), 885-900.  
912 <http://dx.doi.org/10.13031/2013.23153>
- 913 Moriasi, D. N., Rossi, C. G., Arnold, J. G., & Tomer, M. D. (2012). Evaluating hydrology of the  
914 Soil and Water Assessment Tool (SWAT) with new tile drain equations. *Journal of soil and*  
915 *water conservation*, 67(6), 513-524. <https://doi.org/10.2489/jswc.67.6.513>
- 916 Nash, J. E., & Sutcliffe, J. V. (1970). River flow forecasting through conceptual models. Part I—  
917 A discussion of principles. *Journal of hydrology*, 10(3), 282-290.  
918 [http://dx.doi.org/10.1016/0022-1694\(70\)90255-6](http://dx.doi.org/10.1016/0022-1694(70)90255-6)
- 919 Natho-Jina, S., Prasher, S. O., Madramootoo, C. A., & Broughton, R. S. (1987). Measurements  
920 and analysis of runoff from subsurface drained farmlands. *Canadian agricultural engineering*.
- 921 Niu, G.Y., Yang, Z.L., Mitchell, K.E., Chen, F., Ek, M.B., Barlage, M., Kumar, A., Manning, K.,  
922 Niyogi, D., Rosero, E., & Tewari, M. (2011). The community Noah land surface model with  
923 multiparameterization options (Noah-MP): 1. Model description and evaluation with local-  
924 scale measurements. *Journal of Geophysical Research: Atmospheres*, 116(D12).  
925 <https://doi.org/10.1029/2010JD015139>
- 926 Panuska, J. (2020). The Basics of Agricultural Tile Drainage: Basic Engineering Principals  
927 2. *University of Wisconsin-Madison Extension*. Accessed.
- 928 Rahman, M. M., Lin, Z., Jia, X., Steele, D. D., & DeSutter, T. M. (2014). Impact of subsurface  
929 drainage on streamflows in the Red River of the North basin. *Journal of Hydrology*, 511, 474-  
930 483. <https://doi.org/10.1016/j.jhydrol.2014.01.070>

- 931 Ray, D. K., Mueller, N. D., West, P. C., & Foley, J. A. (2013). Yield trends are insufficient to  
932 double global crop production by 2050. *PloS one*, 8(6), e66428.  
933 <https://doi.org/10.1371/journal.pone.0066428>
- 934 Razavi, T., & Coulibaly, P. (2013). Streamflow prediction in ungauged basins: review of  
935 regionalization methods. *Journal of hydrologic engineering*, 18(8), pp.958-975.  
936 [https://doi.org/10.1061/\(ASCE\)HE.1943-5584.0000690](https://doi.org/10.1061/(ASCE)HE.1943-5584.0000690)
- 937 Ritzema, H. P. (1994). Subsurface flow to drains. *Drainage principles and applications*, 16, 263-  
938 304.
- 939 Robinson, M. (1990). *Impact of improved land drainage on river flows*. Institute of Hydrology.
- 940 Robinson, M., & Rycroft, D. W. (1999). The impact of drainage on streamflow. *Agricultural*  
941 *drainage*, 38, 767-800. <https://doi.org/10.2134/agronmonogr38.c23>
- 942 Robinson, M., Ryder, E. L., & Ward, R. C. (1985). Influence on streamflow of field drainage in a  
943 small agricultural catchment. *Agricultural water management*, 10(2), 145-158.  
944 [https://doi.org/10.1016/0378-3774\(85\)90003-4](https://doi.org/10.1016/0378-3774(85)90003-4)
- 945 Saha, S., Moorthi, S., Wu, X., Wang, J., Nadiga, S., Tripp, P., Behringer, D., Hou, Y.T., Chuang,  
946 H.Y., Iredell, M., & Ek, M. (2014). The NCEP climate forecast system version 2. *Journal of*  
947 *climate*, 27(6), pp.2185-2208. <https://doi.org/10.1175/JCLI-D-12-00823.1>
- 948 Sammons, R.J., Mohtar, R.H., & Northcott, W.J. (2005). Modeling subsurface drainage flow of a  
949 tile-drained small watershed using DRAINMOD. *Applied Engineering in Agriculture*, 21(5),  
950 pp.815-834. <http://dx.doi.org/10.13031/2013.19709>
- 951 Schilling, K. E., & Helmers, M. (2008). Effects of subsurface drainage tiles on streamflow in  
952 Iowa agricultural watersheds: Exploratory hydrograph analysis. *Hydrological Processes: An*  
953 *International Journal*, 22(23), 4497-4506. <https://doi.org/10.1002/hyp.7052>
- 954 Schilling, K. E., & Libra, R. D. (2003). Increased baseflow in Iowa over the second half of the  
955 20th century. *JAWRA Journal of the American Water Resources Association*, 39(4), 851-860.  
956 <https://doi.org/10.1111/j.1752-1688.2003.tb04410.x>

957 Schilling, K. E., Jindal, P., Basu, N. B., & Helmers, M. J. (2012). Impact of artificial subsurface  
958 drainage on groundwater travel times and baseflow discharge in an agricultural watershed,  
959 Iowa (USA). *Hydrological Processes*, 26(20), 3092-3100. <https://doi.org/10.1002/hyp.8337>

960 Schottler, S. P., Ulrich, J., Belmont, P., Moore, R., Lauer, J. W., Engstrom, D. R., &  
961 Almendinger, J. E. (2014). Twentieth century agricultural drainage creates more erosive  
962 rivers. *Hydrological processes*, 28(4), 1951-1961. <https://doi.org/10.1002/hyp.9738>

963 Sellami, H., La Jeunesse, I., Benabdallah, S., Baghdadi, N., & Vanclooster, M. (2014).  
964 Uncertainty analysis in model parameters regionalization: a case study involving the SWAT  
965 model in Mediterranean catchments (Southern France). *Hydrology and Earth System*  
966 *Sciences*, 18(6), pp.2393-2413. <https://doi.org/10.5194/hess-18-2393-2014>

967 Singh, R., & Helmers, M. J. (2008). Improving crop growth simulation in the hydrologic model  
968 DRAINMOD to simulate corn yields in subsurface drained landscapes. In *2008 Providence,*  
969 *Rhode Island, June 29–July 2, 2008* (p. 1). American Society of Agricultural and Biological  
970 Engineers. <http://dx.doi.org/10.13031/2013.24598>

971 Singh, R., Archfield, S.A., & Wagener, T. (2014). Identifying dominant controls on hydrologic  
972 parameter transfer from gauged to ungauged catchments—A comparative hydrology approach.  
973 *Journal of Hydrology*, 517, pp.985-996. <http://dx.doi.org/10.1016/j.jhydrol.2014.06.030>

974 Singh, R., Helmers, M. J., & Qi, Z. (2006). Calibration and validation of DRAINMOD to design  
975 subsurface drainage systems for Iowa's tile landscapes. *Agricultural water management*,  
976 85(3), 221-232. <https://doi.org/10.1016/j.agwat.2006.05.013>

977 Singh, R., Helmers, M. J., Crumpton, W. G., & Lemke, D. W. (2007). Predicting effects of  
978 drainage water management in Iowa's subsurface drained landscapes. *Agricultural water*  
979 *management*, 92(3), 162-170. <https://doi.org/10.1016/j.agwat.2007.05.012>

980 Singh, V.P., & Woolhiser, D.A. (2002). Mathematical modeling of watershed hydrology.  
981 *Journal of hydrologic engineering*, 7(4), pp.270-292. [https://doi.org/10.1061/\(ASCE\)1084-  
982 0699\(2002\)7:4\(270\)](https://doi.org/10.1061/(ASCE)1084-0699(2002)7:4(270))

- 983 Skaggs, R. W. (1980). Combination surface-subsurface drainage systems for humid  
984 regions. *Journal of the Irrigation and Drainage Division*, 106(4), 265-283.  
985 <https://doi.org/10.1061/JRCEA4.0001318>
- 986 Skaggs, R. W., Breve, M. A., & Gilliam, J. W. (1994). Hydrologic and water quality impacts of  
987 agricultural drainage\*. *Critical reviews in environmental science and technology*, 24(1), 1-32.  
988 <https://doi.org/10.1080/10643389409388459>
- 989 Skamarock, W. C., & Klemp, J. B. (2008). A time-split nonhydrostatic atmospheric model for  
990 weather research and forecasting applications. *Journal of computational physics*, 227(7),  
991 3465-3485. <https://doi.org/10.1016/j.jcp.2007.01.037>
- 992 Suzuki, K., & Zupanski, M. (2018). Uncertainty in solid precipitation and snow depth prediction  
993 for Siberia using the Noah and Noah-MP land surface models. *Frontiers of Earth Science*,  
994 12(4), pp.672-682. <https://doi.org/10.1007/s11707-018-0691-2>
- 995 Thomas, N. W., Arenas, A. A., Schilling, K. E., & Weber, L. J. (2016). Numerical investigation  
996 of the spatial scale and time dependency of tile drainage contribution to stream flow. *Journal*  
997 *of Hydrology*, 538, 651-666. <http://dx.doi.org/10.1016/j.jhydrol.2016.04.055>
- 998 Tolson, B.A., & Shoemaker, C.A. (2007). Dynamically dimensioned search algorithm for  
999 computationally efficient watershed model calibration. *Water Resources Research*, 43(1).
- 1000 USDA-NASS. (2017). *2017 Census of Agriculture*. <https://doi.org/10.1029/2005WR004723>
- 1001 USDA-NRCS, (2012). Digital general soil map of the United States (STATSGO2). Soil Survey  
1002 Staff, Natural Resources Conservation Service, *United States Department of Agriculture*.
- 1003 Valayamkunnath, P., Barlage, M., Chen, F., Gochis, D. J., & Franz, K. J. (2020). Mapping of 30-  
1004 meter resolution tile-drained croplands using a geospatial modeling approach. *Scientific*  
1005 *data*, 7(1), 1-10. <https://doi.org/10.1038/s41597-020-00596-x>
- 1006 Valayamkunnath, P., Liu, Y., McDaniel, R., & Barlage, M. (2020). RNWMStat: A community-  
1007 contributed R package for evaluating the National Water Model performance in simulating  
1008 streamflow. Release V.0.1 (Version V.0.1). Zenodo. <http://doi.org/10.5281/zenodo.3903720>

- 1009 Wallner, M., Haberlandt, U., & Dietrich, J. (2013). A one-step similarity approach for the  
1010 regionalization of hydrological model parameters based on Self-Organizing Maps. *Journal of*  
1011 *hydrology*, 494, pp.59-71. <http://dx.doi.org/10.1016/j.jhydrol.2013.04.022>
- 1012 Winter, T.C. (2001). The concept of hydrologic landscapes. *JAWRA Journal of the American*  
1013 *Water Resources Association*, 37(2), pp.335-349. [http://dx.doi.org/10.1111/j.1752-](http://dx.doi.org/10.1111/j.1752-1688.2001.tb00973.x)  
1014 [1688.2001.tb00973.x](http://dx.doi.org/10.1111/j.1752-1688.2001.tb00973.x)
- 1015 Wiskow, E., & van der Ploeg, R. R. (2003). Calculation of drain spacings for optimal rainstorm  
1016 flood control. *Journal of Hydrology*, 272(1-4), 163-174. [http://dx.doi.org/10.1016/S0022-](http://dx.doi.org/10.1016/S0022-1694(02)00262-7)  
1017 [1694\(02\)00262-7](http://dx.doi.org/10.1016/S0022-1694(02)00262-7)
- 1018 Wolock, D.M., Winter, T.C., & McMahon, G. (2004). Delineation and evaluation of hydrologic-  
1019 landscape regions in the United States using geographic information system tools and  
1020 multivariate statistical analyses. *Environmental management*, 34(1), pp.S71-S88.  
1021 <https://doi.org/10.1007/s00267-003-5077-9>
- 1022 Xia, Y., Mitchell, K., Ek, M., Sheffield, J., Cosgrove, B., Wood, E., Luo, L., Alonge, C., Wei,  
1023 H., Meng, J., & Livneh, B. (2012). Continental-scale water and energy flux analysis and  
1024 validation for the North American Land Data Assimilation System project phase 2 (NLDAS-  
1025 2): 1. Intercomparison and application of model products. *Journal of Geophysical Research:*  
1026 *Atmospheres*, 117(D3). <https://doi.org/10.1029/2011JD016048>
- 1027 Yang, Y., Anderson, M., Gao, F., Hain, C., Kustas, W., Meyers, T., Crow, W., Finocchiaro, R.,  
1028 Otkin, J., Sun, L., & Yang, Y. (2017). Impact of tile drainage on evapotranspiration in South  
1029 Dakota, USA, based on high spatiotemporal resolution evapotranspiration time series from a  
1030 multisatellite data fusion system. *IEEE Journal of Selected Topics in Applied Earth*  
1031 *Observations and Remote Sensing*, 10(6), pp.2550-2564.  
1032 <https://doi.org/10.1109/JSTARS.2017.2680411>

*Water Resources Research*

Supporting Information for

**Modeling the hydrologic influence of subsurface tile drainage using the National Water Model**

Prasanth Valayamkunnath<sup>a,\*</sup>, David J. Gochis<sup>a</sup>, Fei Chen<sup>a</sup>, Michael Barlage<sup>a</sup>, and Kristie J. Franz<sup>b</sup>

<sup>a</sup>National Center for Atmospheric Research (NCAR), Boulder, Colorado, USA, 80301

<sup>b</sup>Department of Geological and Atmospheric Sciences, Iowa State University, Ames, Iowa, USA, 50011

\* \*Correspondence: Prasanth Valayamkunnath (prasanth@ucar.edu)

**Contents of this file**

Figures S1 to S2

Tables S1 to S3

**Introduction**

In this supporting information, we provide two figures and three tables to support the manuscript. The spatial distributions of land use (i.e., croplands and tile drainage) in the Upper Mississippi River Basin and Ohio River Basin are presented in Figure S1. A graphical explanation for the high-flow and low-flow identification from the streamflow timeseries is presented in Figure S2. All the p-values from the statistical significance tests conducted for the manuscript are provided in Table S1 to S3.

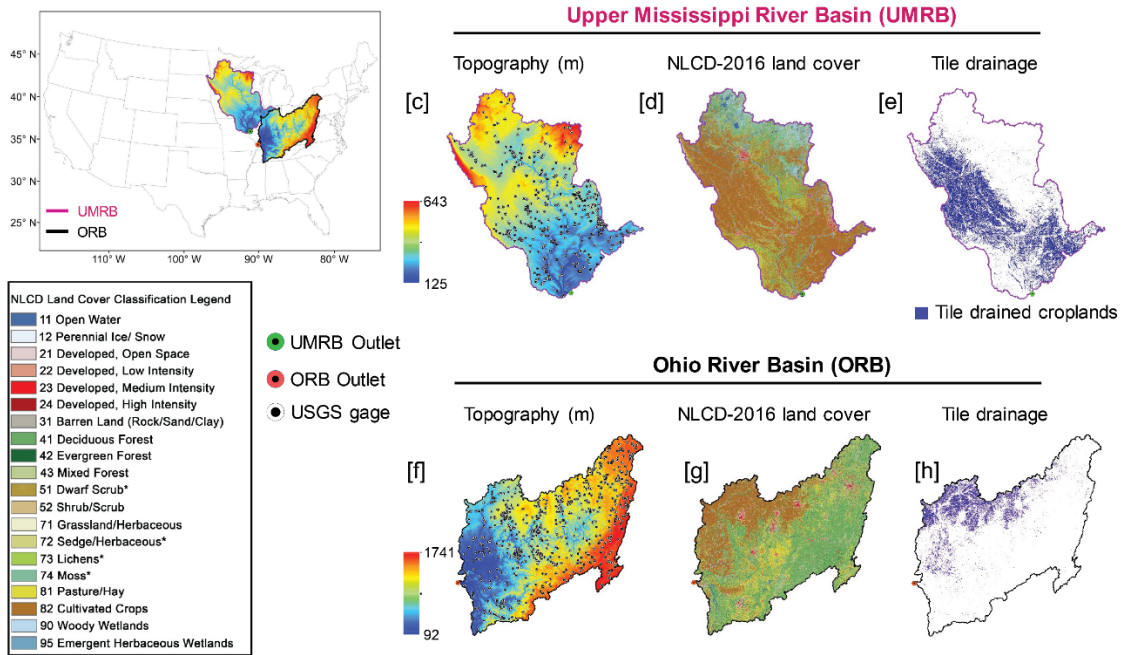


**Figure S1.** The spatial distributions of land use land cover in UMRB and ORB.

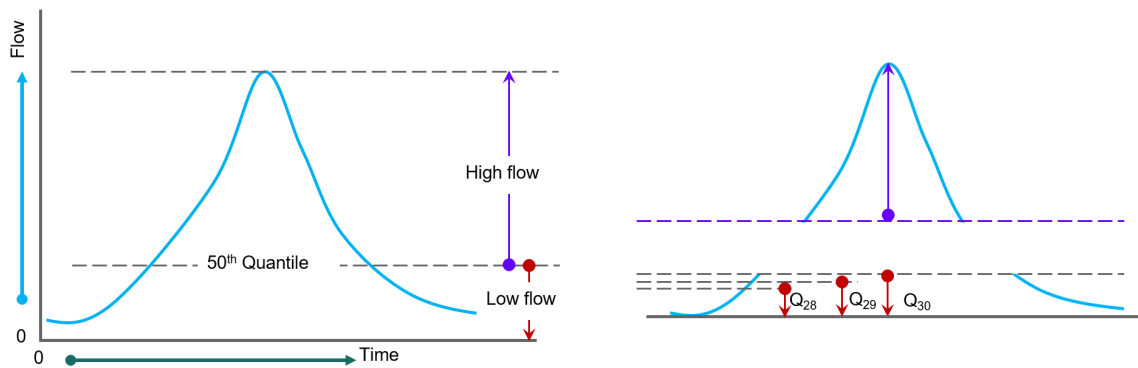


**Figure S2.** Schematic representation of high flow and low flow definitions used in this study.

**Table S1.** The statistical significance (p-value) of the NWM performance change between experiments estimated using Wilcoxon signed rank test for the calibration period. Red font indicates the changes are significant at 0.05 significance level.

<b>Period</b>	<b>Season</b>	<b>Metric</b>	<b>Default [V2.0] and Default [V2.0+TD]</b>	<b>Default [V2.0] and Calibrated [V2.0]</b>	<b>Default [V2.0] and Calibrated [V2.0+TD]</b>	<b>Calibrated [V2.0] and Calibrated [V2.0+TD]</b>
Calibration	DJF	COR	0.0721	0.0000	0.0000	0.4404
Calibration	DJF	RMSE	0.8375	0.3610	0.1896	0.6254
Calibration	DJF	PBIAS	0.8708	0.0000	0.0000	0.1306
Calibration	DJF	NSE	0.1039	0.0000	0.0000	0.0605
Calibration	DJF	NSEWT	0.4115	0.0000	0.0000	0.0557
Calibration	DJF	KGE	0.2201	0.0000	0.0000	0.0951
Calibration	MAM	COR	0.0006	0.0000	0.0000	0.0768
Calibration	MAM	RMSE	0.6055	0.1288	0.1438	0.6006
Calibration	MAM	PBIAS	0.5665	0.0000	0.0000	0.0221
Calibration	MAM	NSE	0.0010	0.0000	0.0000	0.0699
Calibration	MAM	NSEWT	0.0411	0.0000	0.0000	0.0557
Calibration	MAM	KGE	0.0018	0.0000	0.0000	0.2509
Calibration	JJA	COR	0.6105	0.0001	0.0000	0.0189
Calibration	JJA	RMSE	0.8430	0.3390	0.0909	0.3499
Calibration	JJA	PBIAS	0.7664	0.0000	0.0002	0.1101
Calibration	JJA	NSE	0.5618	0.0014	0.0000	0.0035
Calibration	JJA	NSEWT	0.7664	0.0018	0.0000	0.0059
Calibration	JJA	KGE	0.7718	0.0000	0.0000	0.1183
Calibration	SON	COR	0.7990	0.0000	0.0000	0.0994
Calibration	SON	RMSE	0.9831	0.1872	0.0243	0.2912
Calibration	SON	PBIAS	0.9099	0.0000	0.0000	0.0010
Calibration	SON	NSE	0.7881	0.0025	0.0000	0.0049
Calibration	SON	NSEWT	0.9436	0.0006	0.0000	0.0110
Calibration	SON	KGE	0.9492	0.0000	0.0000	0.0189

**Table S2.** The statistical significance (p-value) of the NWM performance change between experiments estimated using Wilcoxon signed rank test for the validation period. Red font indicates the changes are significant at 0.05 significance level.

<b>Period</b>	<b>Season</b>	<b>Metric</b>	<b>Default [V2.0] and Default [V2.0+TD]</b>	<b>Default [V2.0] and Calibrated [V2.0]</b>	<b>Default [V2.0] and Calibrated [V2.0+TD]</b>	<b>Calibrated [V2.0] and Calibrated [V2.0+TD]</b>
Validation	DJF	COR	0.0217	0.0000	0.0000	0.9718
Validation	DJF	RMSE	0.5908	0.0909	0.1644	1.0000
Validation	DJF	PBIAS	0.2509	0.0000	0.0000	0.3799
Validation	DJF	NSE	0.0124	0.0000	0.0000	0.9380
Validation	DJF	NSEWT	0.0135	0.0000	0.0000	0.4531
Validation	DJF	KGE	0.0021	0.0000	0.0001	0.9549
Validation	MAM	COR	0.0008	0.0000	0.0000	0.8763
Validation	MAM	RMSE	0.5859	0.1288	0.1824	0.8486
Validation	MAM	PBIAS	0.8597	0.0000	0.0000	0.2912
Validation	MAM	NSE	0.0031	0.0000	0.0000	0.6868
Validation	MAM	NSEWT	0.0496	0.0000	0.0000	0.3462
Validation	MAM	KGE	0.0005	0.0000	0.0000	0.7025
Validation	JJA	COR	0.3838	0.0000	0.0000	0.0152
Validation	JJA	RMSE	0.8375	0.3799	0.1518	0.5570
Validation	JJA	PBIAS	0.8320	0.0000	0.0000	0.0149
Validation	JJA	NSE	0.4531	0.0003	0.0000	0.0093
Validation	JJA	NSEWT	0.6558	0.0002	0.0000	0.0067
Validation	JJA	KGE	0.5288	0.0000	0.0000	0.5570
Validation	SON	COR	0.8375	0.0000	0.0000	0.1419
Validation	SON	RMSE	0.8875	0.6204	0.4573	0.5908
Validation	SON	PBIAS	0.9718	0.0000	0.0000	0.0332
Validation	SON	NSE	0.8100	0.1458	0.0003	0.0805
Validation	SON	NSEWT	0.8875	0.1039	0.0001	0.0073
Validation	SON	KGE	0.8154	0.0015	0.0000	0.0548

**Table S3.** The statistical significance (p-value) of the NWM performance change between experiments estimated using Wilcoxon signed rank test for the regional simulation. Red font indicate the changes are significant at 0.05 significance level.

<b>Domain</b>	<b>Season</b>	<b>Metric</b>	<b>Default and DefaultTD</b>	<b>Default and Calib</b>	<b>Default and CalibTD</b>	<b>Calib and CalibTD</b>
Regional	DJF	COR	0.0000	0.0000	0.0000	0.0000
Regional	DJF	RMSE	0.3787	0.0508	0.1708	0.8287
Regional	DJF	PBIAS	0.0266	0.0000	0.0000	0.0001
Regional	DJF	NSE	0.0000	0.0000	0.0000	0.1617
Regional	DJF	NSEWT	0.0000	0.0000	0.0000	0.0024
Regional	DJF	KGE	0.0000	0.0000	0.0000	0.0008
Regional	MAM	COR	0.0000	0.0000	0.0000	0.0000
Regional	MAM	RMSE	0.4326	0.2935	0.1369	0.2161
Regional	MAM	PBIAS	0.8638	0.0000	0.0000	0.5096
Regional	MAM	NSE	0.0000	0.0000	0.0000	0.0000
Regional	MAM	NSEWT	0.0000	0.0000	0.0000	0.0001
Regional	MAM	KGE	0.0000	0.0000	0.0000	0.0000
Regional	JJA	COR	0.0731	0.0005	0.0000	0.0000
Regional	JJA	RMSE	0.6772	0.8345	0.0641	0.0276
Regional	JJA	PBIAS	0.9227	0.0000	0.0000	0.0000
Regional	JJA	NSE	0.0409	0.0409	0.0000	0.0000
Regional	JJA	NSEWT	0.1897	0.1200	0.0000	0.0000
Regional	JJA	KGE	0.0339	0.0000	0.0000	0.0000
Regional	SON	COR	0.5707	0.0000	0.0000	0.0000
Regional	SON	RMSE	0.8369	0.9239	0.3731	0.2500
Regional	SON	PBIAS	0.8790	0.0000	0.0000	0.5231
Regional	SON	NSE	0.5348	0.5328	0.0006	0.0027
Regional	SON	NSEWT	0.6718	0.5840	0.0016	0.0003
Regional	SON	KGE	0.4136	0.0000	0.0000	0.0124